i^{2}RES: Integrated Information Relay and Energy Supply Assisted RF Harvesting Communication

Deepak Mishra and Swades De

***Abstract*—To overcome finite lifetime bottleneck in the ubiquitous deployment of low-power wireless devices in Internet-of-Things, we propose a novel Integrated Information Relay and Energy Supply (i^{2}RES) assisted RF harvesting cooperative communication model. i^{2}RES aids the communication between two distant energy-constrained wireless nodes by (i) RF energy transfer to the source and (ii) relaying source data along with supplying energy to the destination. To enable efficient i^{2}RES-powered information transfer to the destination, we first derive and then maximize the delay-limited achievable throughput over Rician channels by jointly optimizing time allocation for information and energy transfer along with relative position of i^{2}RES between source and destination. Although the throughput maximization problem is nonconvex and highly nonlinear, we prove its generalized-convexity and obtain the global-optimal numerical solutions. To gain analytical insights, we also derive tight closed-form approximation for the optimized solutions. Numerical results validate the analysis and demonstrate significant gain in throughput performance via our proposed optimization schemes under practical hardware constraints. Finally, we discuss how the analysis and optimization results can be extended to general RF-EH system settings with relaxed constraints.**

***Index Terms*—Integrated information relay and energy supply, RF energy harvesting, outage analysis, throughput maximization, generalized-convexity, rate-energy tradeoff**

I. Introduction

Controlled energy replenishment via dedicated Radio Frequency (RF) Energy Transfer (ET) has emerged as a promising technique to realize uninterrupted network operation. With the roll-out of 5G and increasing demand for connecting low power wireless devices in Internet of Things (IoT), significance of on-demand wireless energy replenishment of battery-constrained devices has further increased. Among various wireless ET techniques [1], RF-ET has some appealing features, such as, longer range, beamforming capabilities, and joint data and energy transfer provisioning [2]. However, the major bottleneck in the widespread usage of RF-ET technology is its low ET efficiency due to low RF-to-dc rectification efficiency, low energy reception sensitivity [3], and high attenuation owing to path loss and signal dispersion in wireless propagation [1], [2]. So, a lot of attention is being paid to improve the performance of RF-powered networks.

A. State-of-the-Art

1) Smart RF Harvesting Communications: With the advancements in RF Energy Harvesting (EH) circuits [3], output dc voltage and RF-to-dc rectification efficiency have significantly improved. Energy-efficient communications [2] aided by smart antenna technologies [4] and judicious ways of utilizing harvested energy [5] have been proposed to further improve the network performance. Multihop RF-ET schemes providing significant gains by enabling distributed beamforming have been demonstrated experimentally [2] and analytically [6]. Energy sharing based on direct ET using wired power grid [7] and non-direct ET using cooperative transmission [2] helps in overcoming the uncertainty of ambient sources [8].

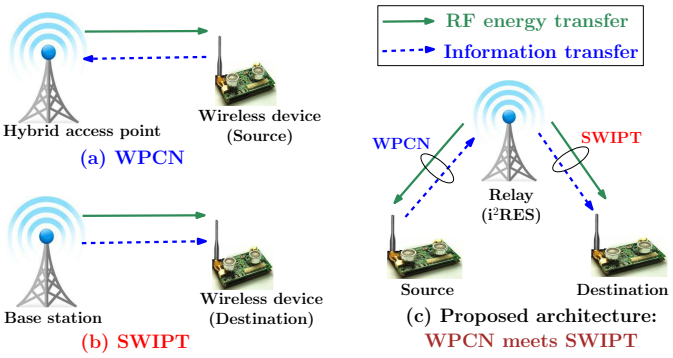

Fig. 1. Architectures for joint wireless energy and information transfer

Improved RF-ET techniques have led to the emergence of Wireless Powered Communication Networks (WPCNs) [9]. Here, as shown in Fig. 1(a), the uplink wireless information transfer (WIT) is powered by the downlink RF-ET from base station or hybrid access point (HAP). To overcome the *doubly-near-far* problem [9] in WPCNs, a *harvest-then-cooperate* protocol was proposed in [10]. Another related field that has gained attention is Simultaneous Wireless Information and Power Transfer (SWIPT) [11], where both energy and information flow are in same direction (see Fig. 1(b)). Practical implementation of SWIPT involves splitting of received signal into two parts: for information decoding and for EH. This signal splitting can be done by either Time Switching (TS), or Power Splitting (PS), or Antenna Switching (AS) [11].

2) Relay-Assisted WPCN and SWIPT: Optimized cooperative relaying [12]–[21] and multiple-input-multiple-output (MIMO) technologies (e.g., [20]) have been recently studied for enabling efficient WPCN and SWIPT. It has been noted that the performance of cooperative relaying is strongly influenced by the relay placement (RP) [2], [6]. Numerical optimal RP solutions in two-hop RF-ET with and without distributed beamforming were studied in [6]. In [22], performance of PS-based SWIPT with multiple randomly deployed EH relays was

D. Mishra and S. De are with the Department of Electrical Engineering and Bharti School of Telecommunication, Indian Institute of Technology Delhi, New Delhi, India (e-mail: {deepak.mishra, swadesd}@ee.iitd.ac.in).

This work has been supported by the Department of Science and Technology (DST) under the grant no. SB/S3/EECE/0248/2014.

studied using stochastic geometry. As the directions for energy and information flow are different in WPCN and SWIPT, their respective performances are studied separately in the literature.

First we discuss the literature on WPCNs. Decode-and-Forward (DF) relay-powered communication with single RF-EH source was studied in [12], [13] for maximizing delay-limited throughput. Optimal time allocations for RF-ET and WIT were investigated in [12] to efficiently utilize the energy available at DF relay. Without direct link, [13] presented numerical solutions for joint optimization of PA and TS. System model with users harvesting energy from RF transmissions of base station and relay nodes for uplink transmission was presented in [14]. A network architecture with dedicated Power Beacons (PBs) overlaid with an exiting cellular network was proposed in [15] for wirelessly-powered information sources and relays. Performance of co-located as well as separately-located access points (APs) and PBs were investigated in [23] and [24]. Authors in [24] also proposed an iterative scheme for minimizing the deployment cost by jointly minimizing the number of optimally located PBs and APs.

We now survey the recent developments on SWIPT where the information relay is powered by the information source. An iterative scheme was proposed in [16] for maximizing end-to-end achievable rate in a multicarrier RF-EH DF relay network. In [17], RF *harvest-and-forward* based Amplify-and-Forward (AF) relaying with multiple antennas was considered, where antenna selection and PS were jointly optimized. Numerical performance of a three-node multi-antenna AF relay system has been recently studied in [18], where the relay simultaneously harvests energy from source and destination. PS and TS based routing protocols were proposed in [19] for RF-EH AF relay system with single source-destination pair. Multi-antenna EH two-hop AF relaying under optimal PS was investigated in [20] for with and without co-channel interference. Apart from these works, joint optimization of PA, RP, and PS in relay-assisted SWIPT to RF-EH destination over line-of-sight (LoS) wireless channels has been recently studied in [21].

B. Research Gap and Motivation

As noted in the literature survey, there has been significant recent interest in the RF-EH research community on optimized cooperative relaying for improving the efficiency of WPCN or SWIPT. The existing works either consider RF-EH relays [10], [16]–[20], or source/relay-powered RF-EH destinations [10], [14], [21], [22], or HAP-powered sources [9]–[13], or the usage of PB for powering sources [15], [23], [24]. *Cooperative RF-EH communication system architecture for powering both energy-constrained source and destination with the help of relay, which can enable perpetual operation of IoT, EH users in small cell networks, and relay-assisted machine-to-machine (M2M) communications, has not been reported in literature. Moreover, to the best of our knowledge, RF-EH cooperative DF relaying protocol, that jointly optimizes throughput performance of WPCN and SWIPT, has not been studied yet.*

Another important observation is that, prior analyses on WPCN and SWIPT operation were done considering Rayleigh fading channel. However, as also noted in [4], [21], the strong LoS component in WPCN and SWIPT cannot be ignored and hence *Rician fading channel model* needs to be considered. Further, while maximizing the efficiency of WPCN or SWIPT, the existing papers present numerical solutions or iterative algorithms. *Closed-form optimal solutions* shedding light on the interplay between different system parameters are mostly missing. Also, as noted in [6], [21], RP plays a significant role in performance of RF-EH networks. However *optimal RP in WPCN*, incorporating the effect of channel randomness on RF-EH, is missing in the literature. Further it is worth noting that, this work is significantly different from [21], which considers DF-relay assisted SWIPT to EH destination with energy-rich source and relay over Rician channels using an available exponential approximation [25] that is valid only for low Rice factor values. Motivated by these observations, we propose a novel relay-powered RF-EH architecture to jointly optimize performance of WPCN and SWIPT over Rician channels.

C. Novelty and Contributions

The key contributions of this work are seven-fold.

- A novel RF-EH cooperative communication system aided by Integrated Information Relay and Energy Supply (i^2RES) is proposed (Fig. 1(c)). It provides energy replenishment to battery-constrained source and destination while relaying their data in a two-hop DF fashion.
- Considering Rician fading, we first obtain a tight exponential approximation for first order Marcum-Q function that holds good even for very high Rice factor. We then derive outage probability in DF relay-powered SWIPT.
- Global-optimal time allocation (TA) for RF-ET and WIT along with optimal RP (position of i^2RES) are obtained to maximize the delay-limited throughput (or minimize outage probability), while satisfying the energy requirements of RF-EH source and destination.
- Global-optimality of the separately and jointly-optimal TA and RP solutions are shown by proving generalized-convexity of the throughput maximization problem.
- Closed-form expressions for the tight analytical approximation of the numerical global-optimal TA and RP are derived to gain insights on the role of system parameters.
- Numerical performance evaluation of the optimized TA and RP solutions are carried out under practical RF-EH system constraints and Rician fading. Also, the tradeoff between achievable throughput and energy demands of source and/or destination is investigated.
- Discussion on extending the results for optimized performance of RF-EH systems with relaxed practical constraints is included to corroborate usefulness of analysis.

D. Scope of the Work

Theoretical challenges addressed in this paper include (i) derivation of closed-form expression for delay-limited throughput in DF relay-powered SWIPT over Rician channels; (ii) generalized convexity proofs for showing global optimality of the proposed solution; and (iii) closed-from expressions for tight approximation of global-optimal TA and RP solutions. The practical scope of theses analytical results, incorporating the real-world constraints of WPCN and SWIPT to enable

the perpetual operation of energy-constrained RF-EH wireless devices in IoT, can be summarized as follows: (1) Closed-form expression for end-to-end signal-to-noise-ratio (SNR) can be used to analyze various performance metrics of WPCN over Rician channels. (2) Optimal TA provides resource allocation policy for jointly optimized WPCN and SWIPT operation. (3) Optimal RP gives insights on the choice for relay deployment and optimal relay selection in multi-relay scenario. (4) Jointly-optimized TA and RP provides bounds on energy requirements that can be met while optimizing relay-powered SWIPT. (5) This work presents benchmark results for optimized WPCN and SWIPT operation which can be extended to study multi-node communication scenarios, that include mobility of nodes and stochastic geometry based analysis. (6) The analysis and optimization results can be easily extended to gain insights on the optimized performance of different RF-EH system models.

II. System Model

Here we present the system model including the considered network topology, channel model, and various stages involved in i^{2}RES-assisted RF-EH cooperative communication.

A. Network Topology and Node Characterization

We consider a three-node RF-EH cooperative communication scenario (cf. Fig. 2), where an energy-constrained source $\mathcal{S}$ communicates with an energy-constrained destination $\mathcal{D}$ via an energy-rich half-duplex DF information relay $\mathcal{R}$. DF relaying protocol is considered because it provides better outage performance as compared to AF relaying at the cost of increased complexity and energy consumption at $\mathcal{R}$. $\mathcal{S}$ and $\mathcal{D}$ are considered as energy-constrained nodes with rechargeable batteries in 5G communication networks or IoT, whereas $\mathcal{R}$ is considered as a PB [15] with data processing and transmission capability. Additionally, $\mathcal{S}$ and $\mathcal{D}$ have RF-EH units for replenishment of their drained battery-energy via RF-ET from $\mathcal{R}$.

$\mathcal{S}$-to-$\mathcal{D}$ direct link is assumed to be unavailable due to large path loss and/or blockage by obstacles. Specially in WPCNs, where the end-to-end communication range is very limited due to the *doubly-near-far* problem [9], low energy reception sensitivity, and ET efficiency [2], [3], energy-constrained $\mathcal{S}$ sends its data to nearby $\mathcal{R}$ for relaying. So in the absence of any obstacle between $\mathcal{S}$ and $\mathcal{D}$, $\mathcal{R}$ can be placed on the direct (linear) path [19] between them or on an elliptical path [21], with $\mathcal{S}$ and $\mathcal{D}$ as the two foci, to come around any obstacle(s).

To enable efficient WPCN and SWIPT in a static three-node topology, we consider the usage of *directional antennas*. $\mathcal{S}$ and $\mathcal{D}$ are equipped with single antenna directed towards $\mathcal{R}$. Although the intended half-duplex operation can be conducted using a single omnidirectional antenna at $\mathcal{R}$, we consider two directional antennas at $\mathcal{R}$ to minimize the dissipation losses in wireless propagation. One antenna is directed towards $\mathcal{S}$ – essentially for efficient RF-powered $\mathcal{S}$-to-$\mathcal{R}$ WIT and the other antenna is directed towards $\mathcal{D}$ for efficient $\mathcal{R}$-to-$\mathcal{D}$ SWIPT.

B. Channel Model and Assumptions

The channels $\mathcal{R}$-to-$\mathcal{S}$ ($h_{\mathcal{RS}}$), $\mathcal{S}$-to-$\mathcal{R}$ ($h_{\mathcal{SR}}$), and $\mathcal{R}$-to-$\mathcal{D}$ ($h_{\mathcal{RD}}$) are assumed statistically independent, with frequency non-selective quasi-static Rician block fading, having respective average powers $\overline{|h_{\mathcal{RS}}|^2} = \frac{a_{\mathcal{RS}} G_{\mathcal{R}} G_{\mathcal{S}}}{\left(d_{\mathcal{SR}}\right)^{\alpha}}$, $\overline{|h_{\mathcal{SR}}|^2} = \frac{a_{\mathcal{SR}} G_{\mathcal{S}} G_{\mathcal{R}}}{\left(d_{\mathcal{SR}}\right)^{\alpha}}$, and $\overline{|h_{\mathcal{RD}}|^2} = \frac{a_{\mathcal{RD}} G_{\mathcal{R}} G_{\mathcal{D}}}{\left(d_{\mathcal{RD}}\right)^{\alpha}}$. α is path loss exponent; $G_{\mathcal{S}}$, $G_{\mathcal{R}}$, and $G_{\mathcal{D}}$ are the antenna gains at $\mathcal{S}$, $\mathcal{R}$, and $\mathcal{D}$; $a_{\mathcal{RS}}$, $a_{\mathcal{SR}}$, and $a_{\mathcal{RD}}$ respectively account for other $\mathcal{R}$-to-$\mathcal{S}$, $\mathcal{S}$-to-$\mathcal{R}$, and $\mathcal{R}$-to-$\mathcal{D}$ channel gain parameters that depend on antenna characteristics and average channel attenuation [26]; $d_{\mathcal{SR}}$ and $d_{\mathcal{RD}}$ are $\mathcal{S}$-to-$\mathcal{R}$ and $\mathcal{R}$-to-$\mathcal{D}$ distances. For reduced signalling overhead at $\mathcal{S}$ and $\mathcal{D}$, we assume the availability of statistics of channel state information (CSI), instead of instantaneous CSI, for all the links at $\mathcal{R}$. They are collected via pilot signals received from $\mathcal{S}$ and $\mathcal{D}$. All optimization related computations are performed at $\mathcal{R}$ using this statistical CSI.

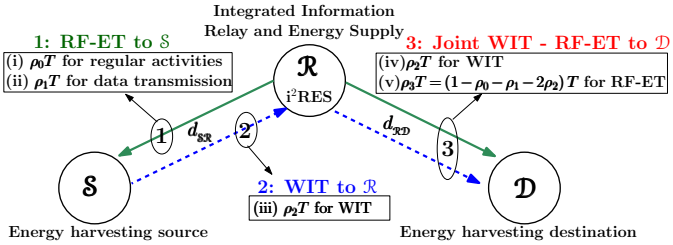

Fig. 2. i^{2}RES-assisted RF harvesting communication system model.

C. i^{2}RES: Integrated Information Relay and Energy Supply

Considering block duration of T sec without any loss of generality, i^{2}RES-assisted RF-EH communication system comprises of the following three main stages (cf. Fig. 2):

- **RF-ET stage** of $(\rho_0 + \rho_1)T$ duration is for the energy replenishment of on-board energy-storage element of $\mathcal{S}$ via RF-ET from $\mathcal{R}$ ($\rho_0 T$: for carrying out regular node activities, such as, sensing, signal-processing, data logging, sleeping, and $\rho_1 T$: for carrying out its information transmission operation). These two separate sub-stages are considered to ensure that the EH node's basic requirements are met by the harvested energy in $\rho_0 T$ duration, before using the remaining harvested energy during $\rho_1 T$ for uplink data transmission.
- **WIT stage** of $\rho_2 T$ duration is dedicated for WIT from $\mathcal{S}$-to-$\mathcal{R}$ using energy harvested during $\rho_1 T$. *Thus, RF-ET and WIT stages jointly represent WPCN operation.*
- **Joint WIT and RF-ET stage** from $\mathcal{R}$-to-$\mathcal{D}$ in the remaining block duration *implements SWIPT*. Here, during $\rho_2 T$ $\mathcal{R}$ forwards the decoded information to $\mathcal{D}$, and $\rho_3 T \triangleq (1 - \rho_0 - \rho_1 \ -2\rho_2)T$ is dedicated for energy replenishment of $\mathcal{D}$ to carryout its regular node operations. We next discuss the operation of each stage in detail.

1) Stages (1) and (2): RF-Powered $\mathcal{S}$-to-$\mathcal{R}$ Communication: During RF-ET stage, $\mathcal{R}$ transmits an RF energy signal x_e in the direction of $\mathcal{S}$. We consider $\mathbb{E}[x_e] = 0$ and $\mathbb{E}\left[|x_e|^2\right] = P_{\mathcal{R}}$, where $P_{\mathcal{R}}$ is the transmit power of $\mathcal{R}$. So the received signal at $\mathcal{S}$, placed $d_{\mathcal{SR}}$ distance away, is given by: $y_{\mathcal{S}} = h_{\mathcal{RS}} x_e + \mathrm{n}_{\mathcal{S}}$, where $\mathrm{n}_{\mathcal{S}}$ is Additive White Gaussian Noise (AWGN) at $\mathcal{S}$.

a) RF energy harvesting at $\mathcal{S}$: We assume that the strength of noise signal $\mathrm{n}_{\mathcal{S}}$ is negligible compared to the

received energy signal $h_{\mathcal{RS}}x_e$, and hence energy harvested from $\mathrm{n}_{\mathcal{S}}$ is neglected. So, amount of energy $E_{\mathcal{S}_0}$ and $E_{\mathcal{S}_1}$ harvested during $\rho_0 T$ and $\rho_1 T$, to be used respectively for regular wireless node activities and information transmission ($\mathcal{S}$-to-$\mathcal{R}$) operation, are given by:

$$E_{\mathcal{S}_j} = \eta_{\mathcal{S}} P_{\mathcal{R}} |h_{\mathcal{RS}}|^2 \rho_j T, \quad \forall j \in \{0,1\} \tag{1}$$

where $\eta_{\mathcal{S}}$ is RF-to-dc rectification efficiency of RF-EH unit at $\mathcal{S}$. We note that, due to the usage of two directional antennas at $\mathcal{R}$ to avoid significant energy dissipation in unintended directions, no energy is harvested at $\mathcal{D}$ and $\mathcal{S}$ respectively during the protocol operation stages 1 and 3.

b) Wireless information transfer from $\mathcal{S}$-to-$\mathcal{R}$: The transmit power $P_{\mathcal{S}}$ of $\mathcal{S}$ using $E_{\mathcal{S}_1}$ is:

$$P_{\mathcal{S}} = \frac{E_{\mathcal{S}_1}}{\rho_2 T} = \eta_{\mathcal{S}} P_{\mathcal{R}} |h_{\mathcal{RS}}|^2 \left(\frac{\rho_1}{\rho_2}\right). \tag{2}$$

With $x_{i_{\mathcal{S}}}$ as the normalized zero mean, unit variance information symbol transmitted by $\mathcal{S}$ and $\mathrm{n}_{\mathcal{R}}$ as the AWGN at $\mathcal{R}$, the corresponding information signal $y_{i_{\mathcal{R}}}$ received at $\mathcal{R}$ due to WIT from $\mathcal{S}$ at transmit power $P_{\mathcal{S}}$ over $\rho_2 T$ duration is:

$$y_{i_{\mathcal{R}}} = h_{\mathcal{SR}} \sqrt{P_{\mathcal{S}}} x_{i_{\mathcal{S}}} + \mathrm{n}_{\mathcal{R}}. \tag{3}$$

2) Stage (3): Joint WIT and RF-ET from $\mathcal{R}$-to-$\mathcal{D}$: From received symbol $y_{i_{\mathcal{R}}}$, $\mathcal{R}$ forwards decoded signal $\widehat{x_{i_{\mathcal{S}}}}$ to $\mathcal{D}$ and simultaneously fulfills its energy requirements by RF-ET.

a) Information decoding at $\mathcal{D}$: With $\mathrm{n}_{\mathcal{D}}$ as AWGN at $\mathcal{D}$, the RF signal received at $\mathcal{D}$ is:

$$y_{i_{\mathcal{D}}} = h_{\mathcal{RD}} \sqrt{P_{\mathcal{R}}} \widehat{x_{i_{\mathcal{S}}}} + \mathrm{n}_{\mathcal{D}}. \tag{4}$$

Here $\mathrm{n}_{\mathcal{S}}$, $\mathrm{n}_{\mathcal{R}}$, and $\mathrm{n}_{\mathcal{D}}$ are considered to be mutually independent with zero mean and variance σ^2. $\rho_2 T$ duration of SWIPT is used for information decoding from $y_{i_{\mathcal{D}}}$. We have considered the same TA fraction ρ_2 for WIT in second and third stages because it helps to simplify the analysis and also because the optimized DF relaying performance can be achieved by controlling the energy allocations and path losses over $\mathcal{R}$-to-$\mathcal{S}$ and $\mathcal{R}$-to-$\mathcal{D}$ links by optimizing TA and RP.

b) RF energy harvesting at $\mathcal{D}$: The remaining block duration $\rho_3 T$ is used for RF-EH at $\mathcal{D}$. With $\rho_3 T = (1-\rho_0-\rho_1-2\rho_2)T$ and $\eta_{\mathcal{D}}$ as RF-to-dc rectification efficiency of RF-EH unit at $\mathcal{D}$, the harvested dc energy $E_{\mathcal{D}}$ to be used for carrying out regular node operation of $\mathcal{D}$ is given by:

$$E_{\mathcal{D}} = \eta_{\mathcal{D}} P_{\mathcal{R}} |h_{\mathcal{RD}}|^2 \rho_3 T. \tag{5}$$

The transmit power at $\mathcal{R}$ is kept fixed at $P_{\mathcal{R}}$ because RF-ET to $\mathcal{S}$ and SWIPT to $\mathcal{D}$ involve ET, which has limited range. This range can be maximized by transmitting at highest power. By optimizing $\rho_0, \rho_1, \rho_2, \rho_3$, we implicitly optimize the available energy resource at $\mathcal{R}$ by allocating energies $(\rho_0+\rho_1)TP_{\mathcal{R}}G_{\mathcal{R}}$ and $(\rho_2+\rho_3)TP_{\mathcal{R}}G_{\mathcal{R}}$ for RF-ET and SWIPT, respectively.

III. Problem Definition

In this section we first obtain a new tight analytical approximation for the first order Marcum-Q function that holds good even for very high values of Rice factor. Using this proposed approximation, we derive closed-form outage probability expressions for WPCN and RF-powered DF-relay assisted SWIPT over Rician channels. Finally, we present the mathematical formulation for throughput maximization problem by accounting the practical RF-EH system constraints.

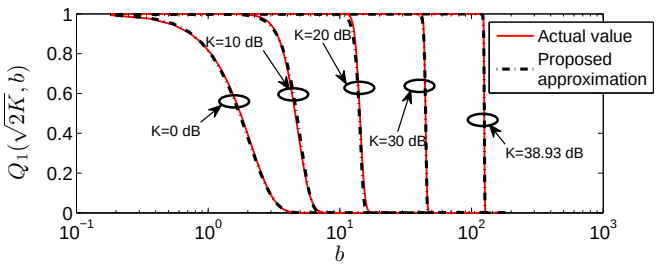

Fig. 3. Validation of approximation for $Q_1(\sqrt{2K}, b)$ with varying K and b.

A. Exponential Approximation for Analyzing Rician Channels with Strong LoS Component

For Rician fading channel model, instantaneous SNR γ follows the weighted noncentral-χ^2 distribution with two degrees of freedom; its cumulative distribution function (CDF) is [27]:

$$F_{\gamma}(x) = \Pr[\gamma \le x] = 1 - Q_1\left(\sqrt{2K}, \sqrt{2(1+K)x/\overline{\gamma}}\right) \tag{6}$$

where $Q_1(\cdot,\cdot)$ is the first order Marcum Q-function [27], $\overline{\gamma}$ is average SNR, and Rice factor K is the ratio of power of LoS component to the scattered components. As both $\mathcal{R}$-to-$\mathcal{S}$ and $\mathcal{R}$-to-$\mathcal{D}$ links are used for RF-ET and have similar communication range, we consider the same K over all links [4], [21], [28]. For analytical insights on performance of i^{2}RES-assisted communication over Rician channels, we note a tight exponential-type approximation [25] for $Q_1(\cdot,\cdot)$:

$$Q_1(a,b) \approx \exp\left(-e^{\phi(a)} b^{\varphi(a)}\right). \tag{7}$$

Here $\phi(a)$ and $\varphi(a)$ are functions of a, and are conditionally defined for $a \ll 1$ and $1 \le a \le 6$ in [25]. Its reliability and goodness have been validated in recent papers [21], [25] for Rice factor $K \le 10$. However, the approximation in (7) does not hold for $K > 10$, i.e., for $a = \sqrt{2K} > 5$. So, for accounting the effect of high Rice factor values up to $K = 39$ dB in RF-ET process, we obtain polynomial expressions for $\phi(a)$ and $\varphi(a)$, along the similar to lines as in [25]. Our proposed polynomial expressions for $\phi(a)$ and $\varphi(a)$, given below, hold good for $1 \le K \le 8000$:

$$\begin{aligned}\phi(a) \triangleq &-3.0888\times10^{-10}a^6 + 1.8362\times10^{-7}a^5 \\ &- 3.7185\times10^{-5}a^4 + 3.4103\times10^{-3}a^3 \\ &- 0.1624a^2 - 1.4318a + 0.7409,\end{aligned} \tag{8a}$$

$$\begin{aligned}\varphi(a) \triangleq\ & 5.1546\times10^{-11}a^6 - 3.1961\times10^{-8}a^5 + \\ & 6.3859\times10^{-6}a^4 - 5.4159\times10^{-4}a^3 + \\ & 1.9833\times10^{-2}a^2 + 0.9044a + 0.9439.\end{aligned} \tag{8b}$$

The goodness of proposed approximation for varying K can be observed from Fig. 3. Root mean square error (RMSE) of less than 0.005 in the approximation also validates its quality and reliability. We use this approximation to derive closed-form expression for the outage probability.

B. Outage Probability Analysis

As there is no direct $\mathcal{S}$-to-$\mathcal{D}$ link available, the end-to-end SNR γ_{E2E} is limited by the lower of $\mathcal{S}$-to-$\mathcal{R}$ SNR $\gamma_{\mathcal{SR}}$ and $\mathcal{R}$-to-$\mathcal{D}$ SNR $\gamma_{\mathcal{RD}}$, i.e., $\gamma_{E2E} = \min\{\gamma_{\mathcal{SR}}, \gamma_{\mathcal{RD}}\}$. Using (2), (3), (4), the received SNRs $\gamma_{\mathcal{SR}}$ and $\gamma_{\mathcal{RD}}$ are given as:

$$\gamma_{\mathcal{SR}} = \frac{\rho_1 \eta_{\mathcal{S}} P_{\mathcal{R}}}{\rho_2 \sigma^2} |h_{\mathcal{RS}}|^2 \times |h_{\mathcal{SR}}|^2,\ \gamma_{\mathcal{RD}} = \frac{P_{\mathcal{R}}}{\sigma^2} |h_{\mathcal{RD}}|^2. \quad (9)$$

Using (9), (6), (7), the complimentary CDF (CCDF) of received SNR $\gamma_{\mathcal{RD}}$ at $\mathcal{D}$ is given by:

$$\Pr[\gamma_{\mathcal{RD}} > x] = e^{-\mathcal{C}_2 x^{\mathcal{B}} \left(d_{\mathcal{RD}}\right)^{\mathcal{B}\alpha}}, \quad (10)$$

with $\mathcal{C}_2 \triangleq \mathcal{A}\left(\frac{2(1+K)\sigma^2}{P_{\mathcal{R}} a_{\mathcal{RD}} G_{\mathcal{R}} G_{\mathcal{D}}}\right)^{\mathcal{B}}$, $\mathcal{A} = e^{\phi\left(\sqrt{2K}\right)}$, $\mathcal{B} = \frac{\varphi\left(\sqrt{2K}\right)}{2}$. Similarly, using $\Pr\left[|h_{\mathcal{RS}}|^2 > x\right] = e^{-\mathcal{A}\left(\frac{2(1+K)x\left(d_{\mathcal{SR}}\right)^{\alpha}}{a_{\mathcal{RS}} G_{\mathcal{R}} G_{\mathcal{S}}}\right)^{\mathcal{B}}}$, $\Pr\left[|h_{\mathcal{SR}}|^2 > x\right] = e^{-\mathcal{A}\left(\frac{2(1+K)x\left(d_{\mathcal{SR}}\right)^{\alpha}}{a_{\mathcal{SR}} G_{\mathcal{S}} G_{\mathcal{R}}}\right)^{\mathcal{B}}}$ due to Rician fading channel assumption and applying approximation (7), the CCDF of $\gamma_{\mathcal{SR}}$, which involves product of two independent random variables $\sqrt{\frac{\rho_1 \eta_{\mathcal{S}} P_{\mathcal{R}}}{\rho_2 \sigma^2}} |h_{\mathcal{RS}}|^2$ and $\sqrt{\frac{\rho_1 \eta_{\mathcal{S}} P_{\mathcal{R}}}{\rho_2 \sigma^2}} |h_{\mathcal{SR}}|^2$, is:

$$\begin{aligned}\Pr[\gamma_{\mathcal{SR}} > x] &= \int_0^{\infty} \Pr\left[\sqrt{\frac{\rho_1 \eta_{\mathcal{S}} P_{\mathcal{R}}}{\rho_2 \sigma^2}} |h_{\mathcal{SR}}|^2 \le \frac{x}{y}\right] \\ &\quad \times \frac{\partial}{\partial y}\left(\Pr\left[\sqrt{\frac{\rho_1 \eta_{\mathcal{S}} P_{\mathcal{R}}}{\rho_2 \sigma^2}} |h_{\mathcal{RS}}|^2 \le y\right]\right) dy \\ &= \mathcal{C}_1 \left(\frac{\rho_2 x}{\rho_1} d_{\mathcal{SR}}^{2\alpha}\right)^{\frac{\mathcal{B}}{2}} \mathbf{K_1}\left(\mathcal{C}_1 \left(\frac{\rho_2 x}{\rho_1} d_{\mathcal{SR}}^{2\alpha}\right)^{\frac{\mathcal{B}}{2}}\right) \quad (11)\end{aligned}$$

where $\mathcal{C}_1 \triangleq 2\mathcal{A}\left(\frac{2(1+K)}{G_{\mathcal{S}} G_{\mathcal{R}}} \sqrt{\frac{\sigma^2}{\eta_{\mathcal{S}} P_{\mathcal{R}} a_{\mathcal{RS}} a_{\mathcal{SR}}}}\right)^{\mathcal{B}}$, and $\mathbf{K_1}(\cdot)$ is the first order modified Bessel function of second kind.

The independence of $h_{\mathcal{RS}}$ and $h_{\mathcal{SR}}$ is considered because channel reciprocity of uplink WIT from an EH battery-constrained $\mathcal{S}$ and downlink ET from an energy rich $\mathcal{R}$ is difficult realize in practice [10], [29], [30]. This is due to the fact that baseband-to-baseband channel between $\mathcal{S}$ and $\mathcal{R}$ is not necessarily reciprocal as they have different phase, frequency, and energy characteristics in antennas associated with their respective transmit and receive chains [31].

The outage probability p_{out}, defined under path loss and Rician fading, is the probability that the received data rate at $\mathcal{D}$ from $\mathcal{S}$ via $\mathcal{R}$ falls below a threshold R. Mathematically, p_{out} as a function of TA $\boldsymbol{\rho} = \{\rho_0, \rho_1, \rho_2, \rho_3\}$ and i^{2}RES position (RP) $\boldsymbol{d} = \{d_{\mathcal{SR}}, d_{\mathcal{RD}}\}$ is given by:

$$\begin{aligned}p_{out} &= \Pr\left(\rho_2 \log_2(1+\gamma_{E2E}) < R\right) \\ &= \Pr\left(\min\{\gamma_{\mathcal{SR}}, \gamma_{\mathcal{RD}}\} < 2^{\frac{R}{\rho_2}} - 1\right) \\ &= 1 - \Pr\left(\gamma_{\mathcal{SR}} > 2^{\frac{R}{\rho_2}} - 1\right) \Pr\left(\gamma_{\mathcal{RD}} > 2^{\frac{R}{\rho_2}} - 1\right) \\ &= 1 - e^{-\mathcal{C}_2\left(2^{\frac{R}{\rho_2}}-1\right)^{\mathcal{B}} \left(d_{\mathcal{RD}}\right)^{\mathcal{B}\alpha}} \left(\frac{\rho_2}{\rho_1}\left(2^{\frac{R}{\rho_2}} - 1\right)\right)^{\frac{\mathcal{B}}{2}} \times \\ &\quad \mathcal{C}_1 \left(d_{\mathcal{SR}}\right)^{\mathcal{B}\alpha} \mathbf{K_1}\left(\mathcal{C}_1 \left(d_{\mathcal{SR}}\right)^{\mathcal{B}\alpha} \left(\frac{\rho_2}{\rho_1}\left(2^{\frac{R}{\rho_2}} - 1\right)\right)^{\frac{\mathcal{B}}{2}}\right) \quad (12)\end{aligned}$$

Outage expression derived in (12) has a lot of practical applicability. Closed-form expression for p_{out} in conventional WPCN over Rician channels with K as high as 39 dB can be obtained using (11) and (12). Further, (12) also holds for Rayleigh fading case. The corresponding outage probability can be obtained by substituting $K = 0$, $\mathcal{A} = \frac{1}{2}$, and $\mathcal{B} = 1$.

We consider a rate-constrained communication scenario, where the delay-limited throughput [19] is given by the source transmission rate R multiplied by the probability of achieving this rate at the receiver. Mathematically, $\tau = R \times \Pr\left(\rho_2 \log_2(1+\gamma_{E2E}) \ge R\right)$. So, using p_{out} given by (12), throughput τ for i^{2}RES-assisted communication is given by:

$$\tau \triangleq R(1 - p_{out}). \quad (13)$$

Given τ as a function of TA $\boldsymbol{\rho} = \{\rho_0, \rho_1, \rho_2, \rho_3\}$ for RF-ET and WIT, along with RP $\boldsymbol{d} = \{d_{\mathcal{SR}}, d_{\mathcal{RD}}\}$, for typical relay transmit power $P_{\mathcal{R}}$ and practical system parameters $a_{\mathcal{RS}}$, $a_{\mathcal{SR}}$, $a_{\mathcal{RD}}$, $G_{\mathcal{S}}, G_{\mathcal{R}}, G_{\mathcal{D}}$, α, K, $\eta_{\mathcal{S}}$, $\eta_{\mathcal{D}}$, R, σ^2, we intend to find the optimal $\boldsymbol{\rho}^*$ and $\boldsymbol{d}^*$ that maximizes τ (or minimizes p_{out}), while satisfying energy demands of $\mathcal{S}$ and $\mathcal{D}$.

C. Throughput Maximization Problem (TMP) Formulation

The TMP with τ as objective and $\boldsymbol{\rho}$ and $\boldsymbol{d}$ as optimization variables can be formulated as:

$$\begin{aligned}&\textbf{TMP}: \underset{\rho_0,\rho_1,\rho_2,\rho_3,d_{\mathcal{SR}},d_{\mathcal{RD}}}{\text{maximize}} \quad \tau, \quad \text{subject to:} \\ &C1: \zeta_{E\mathcal{S}} \le \frac{\mathbb{E}\left[E_{\mathcal{S}_0}\right]}{T}, \qquad C2: \zeta_{E\mathcal{D}} \le \frac{\mathbb{E}\left[E_{\mathcal{D}}\right]}{T}, \\ &C3: \max\{P_{\mathcal{S}}\} \le \frac{\text{EIRP}_{\max}}{G_{\mathcal{S}}}, \quad C4: \rho_j \le 1,\ \forall \rho_j \in \boldsymbol{\rho}, \\ &C5: \rho_j \ge 0,\ \forall \rho_j \in \boldsymbol{\rho}, \qquad C6: d_{\mathcal{SR}} \ge d_{\min}, \\ &C7: d_{\mathcal{RD}} \ge d_{\min}, \qquad C8: d_{\mathcal{SR}} + d_{\mathcal{RD}} \ge D + \delta.\end{aligned} \quad (14)$$

In (14), $\zeta_{E\mathcal{S}}$ and $\zeta_{E\mathcal{D}}$ are normalized energy requirements at $\mathcal{S}$ and $\mathcal{D}$ in a block duration T, for their respective perpetual operation. They actually represent the minimum average harvested energy required per block duration [24], [32]. $\frac{\mathbb{E}\left[E_{\mathcal{S}_0}\right]}{T} = \frac{\rho_0 \eta_{\mathcal{S}} a_{\mathcal{RS}} P_{\mathcal{R}} G_{\mathcal{R}} G_{\mathcal{S}}}{\left(d_{\mathcal{SR}}\right)^{\alpha}}$, $\frac{\mathbb{E}\left[E_{\mathcal{D}}\right]}{T} = \frac{\rho_3 \eta_{\mathcal{D}} a_{\mathcal{RD}} G_{\mathcal{R}} G_{\mathcal{D}} P_{\mathcal{R}}}{\left(d_{\mathcal{RD}}\right)^{\alpha}}$, and $\mathbb{E}[P_{\mathcal{S}}] = \frac{\rho_1 \eta_{\mathcal{S}} a_{\mathcal{RS}} P_{\mathcal{R}} G_{\mathcal{R}} G_{\mathcal{S}}}{\rho_2 \left(d_{\mathcal{SR}}\right)^{\alpha}}$. $\text{EIRP}_{\max}$ in $C3$ is the maximum Effective Isotropic Radiated Power (EIRP) limit defined by the FCC regulations for transmission in Industrial, Scientific and Medical (ISM) bands [33]. The constraint $C3$ ensures that the maximum transmit power $P_{\mathcal{S}}$ of $\mathcal{S}$ is below the maximum permissible limit. As $P_{\mathcal{S}}$ is a random variable following noncentral-χ^2 distribution, $C3$ can be ensured by: $\Pr\left[P_{\mathcal{S}} > \frac{\text{EIRP}_{\max}}{G_{\mathcal{S}}}\right] < \epsilon$, where the tolerance $\epsilon \ll 1$. After using the approximation (7) and applying some simplifications, $C3$ reduces to $\mathbb{E}[P_{\mathcal{S}}] \le \frac{\mathcal{Y}\,\text{EIRP}_{\max}}{G_{\mathcal{S}}}$, where $\mathcal{Y} \triangleq 2(1+K)\left(\frac{\mathcal{A}}{\ln\left(\frac{1}{\epsilon}\right)}\right)^{\frac{1}{\mathcal{B}}}$. We set $\epsilon = 10^{-3}$. In $C6$ and $C7$, $d_{\min} = \frac{2L^2}{\lambda}$ is the minimum $\mathcal{S}$-to-$\mathcal{R}$ or $\mathcal{R}$-to-$\mathcal{D}$ distance requirement for their antennas to be in radiating far-field region [34]. $C6$ and $C7$ help in modeling the distance-based received power variation that holds for far-field region [26, Section 2.6] to avoid the scattering phenomena in the antenna

near-field. Here L is the largest antenna dimension and λ is the wavelength of the transmitted RF signal. δ in $C8$ defines the trajectory or path for RP between $\mathcal{S}$ and $\mathcal{D}$, placed D distance apart, depending on the presence of obstacles. If there are no obstacles, then $\delta = 0$ as $\mathcal{R}$ can be placed on the LoS path between $\mathcal{S}$ and $\mathcal{D}$. Otherwise $\delta > 0$. If $\mathcal{R}$ is placed on elliptical path [21], with $\mathcal{S}$ and $\mathcal{D}$ as the two foci, to come around the obstacle, then $\delta = \frac{D(1-\varepsilon)}{\varepsilon}$, where $\varepsilon \leq 1$ is the eccentricity of ellipse. Although elliptical topology is considered, any other RP topology satisfying the basic property where $\mathcal{S}$-to-$\mathcal{R}$ distance increases with decreased $\mathcal{R}$-to-$\mathcal{D}$ distance can also be employed. From (13) and (14) it may be noted that, for a fixed transmission rate R, TMP is equivalent to the problem of minimizing p_{out} subject to constraints $C1$–$C8$. TMP is infeasible if the energy demands $\zeta_{E\mathcal{S}}$ and $\zeta_{E\mathcal{D}}$ cannot be met even by the joint global-optimal TA and RP solution $(\boldsymbol{\rho^*, d^*})$.

IV. Optimal Time Allocation and i^{2}RES Placement

In this section we obtain individual and joint global-optimal TA and RP solutions for TMP.

A. Optimal Time Allocation for ET and WIT with Fixed RP

First, we consider a practical scenario where i^{2}RES or $\mathcal{R}$ is connected to a power grid such that its location $\boldsymbol{d}$ cannot be changed. In such a setting, to enable efficient RF-powered SWIPT from $\mathcal{S}$ to $\mathcal{D}$ via $\mathcal{R}$, we obtain optimal TA $\boldsymbol{\rho}^*$ for a given RP $\boldsymbol{d} = \{d_{\mathcal{SR}}, d_{\mathcal{RD}}\}$. Since ρ_0 in constraint $C1$ does not exist explicitly in the objective function τ expression, TMP for a fixed RP is maximized when ρ_0 takes the minimum value, just enough to meet $C1$. In other words, optimal ρ_0, denoted by ρ_0^*, obtained by solving $C1$ at strict equality, is given by:

$$\rho_0^* = \frac{\zeta_{E\mathcal{S}} \left(d_{\mathcal{SR}}\right)^{\alpha}}{\eta_{\mathcal{S}} a_{\mathcal{RS}} P_{\mathcal{R}} G_{\mathcal{R}} G_{\mathcal{S}}}. \tag{15}$$

Similarly TA ρ_3, used for RF-EH at $\mathcal{D}$ via SWIPT from $\mathcal{R}$, also does not contribute to τ. So for maximizing τ, optimal ρ_3, representing minimum EH time sufficient for meeting energy demands of $\mathcal{D}$, obtained by solving $C2$ at strict equality is:

$$\rho_3^* = 1 - \rho_0^* - \rho_1^* - 2\rho_2^* = \frac{\zeta_{E\mathcal{D}} \left(d_{\mathcal{RD}}\right)^{\alpha}}{\eta_{\mathcal{D}} a_{\mathcal{RD}} G_{\mathcal{R}} G_{\mathcal{D}} P_{\mathcal{R}}}. \tag{16}$$

Using (16), we next represent optimal ρ_1 in terms of ρ_2^* as:

$$\rho_1^* = 1 - 2\rho_2^* - \frac{\zeta_{E\mathcal{S}} \left(d_{\mathcal{SR}}\right)^{\alpha}}{\eta_{\mathcal{S}} a_{\mathcal{RS}} P_{\mathcal{R}} G_{\mathcal{R}} G_{\mathcal{S}}} - \frac{\zeta_{E\mathcal{D}} \left(d_{\mathcal{RD}}\right)^{\alpha}}{\eta_{\mathcal{D}} a_{\mathcal{RD}} G_{\mathcal{R}} G_{\mathcal{D}} P_{\mathcal{R}}}. \tag{17}$$

Let $\rho_{ET}^* \triangleq \rho_0^* + \rho_3^*$ be the optimal ET time allocated for meeting energy demands of $\mathcal{S}$ and $\mathcal{D}$. Using (15), (16), (17) in (14), TMP with fixed RP, denoted by TMP-TA, is given as:

$$\begin{aligned} \textbf{TMP-TA}: \quad & \underset{\rho_2}{\text{maximize}} \quad \tau \\ \text{subject to:} \quad & C9: \frac{\left(1 - 2\rho_2 - \rho_{ET}^*\right) \eta_{\mathcal{S}} a_{\mathcal{RS}} P_{\mathcal{R}} G_{\mathcal{R}} G_{\mathcal{S}}^2}{\rho_2 \left(d_{\mathcal{SR}}\right)^{\alpha} \mathcal{Y}\, \text{EIRP}_{\max}} \leq 1, \\ & C10: \rho_2 \leq 1/2, \qquad C11: \rho_2 \geq 0. \end{aligned} \tag{18}$$

Here $C9$ is obtained by substituting ρ_{ET}^* in $C3$ of TMP. Notice that although TMP is non-convex, the transformed equivalent single-variable (WIT time ρ_2) problem TMP-TA due to its generalized-convexity [35] in ρ_2 for a fixed RP has a unique global-optimal solution ρ_2^*, obtained by solving the Karush-Kuhn-Tucker (KKT) conditions [36]. This result is presented in Theorem 1. Before that, we present the formal definition of a pseudoconcave function and a result stating that the KKT conditions are satisfied at its unique global-maximum.

Definition 1: A differentiable function f: $\mathbb{R}^n \to \mathbb{R}$, defined on a nonempty open convex set Ω, is called pseudoconcave if $\forall\ x, y \in \Omega$ with $x \neq y$, $\nabla f(x)^{\intercal}(y - x) \leq 0 \implies f(x) \geq f(y)$. A pseudoconcave function f defined over a convex set has a similar property as in case of concave functions, which states that, its local maximum is also the global maximum [36].

Lemma 1: (Corollary to [36, Theorem 4.3.8]) Consider a constraint maximization problem **(P)** with an objective function to be maximized over a feasible region S being pseudoconcave at $\overline{x} \in S$, constraint functions are differentiable and quasiconvex at $\overline{x}$, and KKT conditions hold at $\overline{x}$. Then $\overline{x}$ is the global optimal solution providing the maximum value.

Theorem 1: As the objective function τ to be maximized in TMP-TA is pseudoconcave in ρ_2, the differentiable constraint $C9$ is convex, and the constraints $C10$–$C11$ are affine, the global-optimal TA ρ_2^* is obtained by solving KKT conditions.

Proof: See Appendix A. ∎

Considering $C9$ while keeping the boundary constraints $C10$–$C11$ implicit, the Lagrangian function of TMP-TA is: $\mathcal{L}_{\rho} = \tau - \mu \left[\left(1 - 2\rho_2 - \rho_{ET}^*\right) \frac{\eta_{\mathcal{S}} a_{\mathcal{RS}} P_{\mathcal{R}} G_{\mathcal{R}} G_{\mathcal{S}}^2}{\rho_2 \left(d_{\mathcal{SR}}\right)^{\alpha} \mathcal{Y}\, \text{EIRP}_{\max}} - 1 \right]$, where μ is the Lagrange multiplier associated with constraint $C9$. Using (15), (17), and Lagrangian function $\mathcal{L}_{\rho}$, we solve the following two KKT conditions, while satisfying the primal feasibility constraints $C9$–$C11$ and dual feasibility constraint $\mu \geq 0$, to find KKT point $(\rho_0^*, \rho_1^*, \rho_2^*, \rho_3^*, \mu^*)$ of TMP-TA.

$$\frac{\partial \mathcal{L}_{\rho}}{\partial \rho_2} = \mathcal{G}_1 \mathcal{G}_2 + \mu \frac{\left(1 - \rho_{ET}^*\right) \eta_{\mathcal{S}} a_{\mathcal{RS}} P_{\mathcal{R}} G_{\mathcal{R}} G_{\mathcal{S}}^2}{\rho_2^2 \left(d_{\mathcal{SR}}\right)^{\alpha} \mathcal{Y}\, \text{EIRP}_{\max}} = 0, \tag{19a}$$

$$\mu \left[\left(1 - 2\rho_2 - \rho_{ET}^*\right) \frac{\eta_{\mathcal{S}} a_{\mathcal{RS}} P_{\mathcal{R}} G_{\mathcal{R}} G_{\mathcal{S}}^2}{\rho_2 \left(d_{\mathcal{SR}}\right)^{\alpha} \mathcal{Y}\, \text{EIRP}_{\max}} - 1 \right] = 0. \tag{19b}$$

$\mathcal{G}_1$ and $\mathcal{G}_2$ in (19a), representing $\frac{\partial \tau}{\partial \rho_2} = \mathcal{G}_1 \mathcal{G}_2$, are defined as:

$$\mathcal{G}_1 \triangleq \frac{\mathcal{C}_1 \left(\frac{\rho_2}{\rho_1} \left(2^{\frac{R}{\rho_2}} - 1\right) d_{\mathcal{SR}}^{2\alpha} \right)^{\frac{\mathcal{B}}{2}} e^{-\mathcal{C}_2 \left(2^{\frac{R}{\rho_2}} - 1\right)^{\mathcal{B}} \left(d_{\mathcal{RD}}\right)^{\mathcal{B}\alpha}}}{2\rho_2^2 \left(1 - 2\rho_2 - \rho_{ET}^*\right) \left(2^{\frac{R}{\rho_2}} - 1\right)}, \tag{20a}$$

$$\begin{aligned} \mathcal{G}_2 \quad \triangleq \quad & 2^{\frac{R}{\rho_2}+1} \left(2^{\frac{R}{\rho_2}} - 1\right)^{\mathcal{B}} R \ln(2) \left(1 - \rho_{ET}^* - 2\rho_2\right) \times \\ & \mathcal{C}_2 \left(d_{\mathcal{RD}}\right)^{\mathcal{B}\alpha} \mathbf{K_1}(\mathcal{Z}) - \left[\rho_2 \left(1 - \rho_{ET}^*\right) \left(2^{\frac{R}{\rho_2}} - 1\right) \right. \\ & \left. - 2^{\frac{R}{\rho_2}} R \ln(2) \left(1 - \rho_{ET}^* - 2\rho_2\right) \right] \mathcal{Z}\, \mathbf{K_0}(\mathcal{Z}), \end{aligned} \tag{20b}$$

with $\mathcal{Z} \triangleq \mathcal{C}_1 d_{\mathcal{SR}}^{\mathcal{B}\alpha} \left(\frac{\rho_2}{\rho_1} \left(2^{\frac{R}{\rho_2}} - 1\right) \right)^{\frac{\mathcal{B}}{2}}$. Note that, $\rho_2 \neq \{0, \frac{1}{2}\}$ to have a positive τ, because some time is needed for RF-ET (ρ_0, ρ_1, ρ_3) and WIT (ρ_2). Hence, $C10$–$C11$ can be kept implicit because they are never satisfied at strict equality.

As τ is pseudoconcave in ρ_2 (see Theorem 1), maximum τ is given by the *critical* point $\rho_{2,C}$ (if it exists in the feasible

region defined by $C9$–$C11$), where the gradient of τ vanishes, i.e., $\frac{\partial\tau(\rho_{2,C})}{\partial\rho_2}=0$. This implies that, if $\mu=0$ in (19a) the optimal TA $\rho_2^*=\rho_{2,C}$ is obtained by solving $\mathcal{G}_1\mathcal{G}_2=0$. However, as $\mathcal{G}_1\neq 0\;\forall\,0<\rho_2<\frac{1}{2}$ and τ is pseudoconcave in ρ_2 (see Appendix A) with $\tau=0$ for $\rho_2=\left\{0,\frac{1}{2}\right\}$, we note that $\rho_{2,C}\triangleq\{\rho_2\mid\mathcal{G}_2=0\}<\frac{1}{2}$. Secondly with $\mu>0$, ρ_2^* is given by *boundary* point $\rho_{2,B}$ obtained by solving $C9$ at equality:

$$\rho_{2,B}=\frac{\eta_{\mathcal{S}}\,a_{\mathcal{RS}}P_{\mathcal{R}}G_{\mathcal{R}}G_{\mathcal{S}}^2\left(1-\rho_{ET}^*\right)}{2\eta_{\mathcal{S}}\,a_{\mathcal{RS}}P_{\mathcal{R}}G_{\mathcal{R}}G_{\mathcal{S}}^2+\left(d_{\mathcal{SR}}\right)^{\alpha}\mathcal{Y}\,\mathrm{EIRP}_{\max}}. \tag{21}$$

$\rho_{2,B}<\frac{1}{2}$ actually represents the *minimum proportion ρ_2 of time that can be allocated for WIT (or maximum proportion ρ_1 for RF-ET)* such that EIRP from $\mathcal{R}$ to $\mathcal{S}$ is below $\mathrm{EIRP}_{\max}$. Finally, $\mu^*=\mu_B>0$ for $\rho_2^*=\rho_{2,B}$, obtained using (19a), is:

$$\mu_B\triangleq-\frac{\rho_{2,B}^2\left(d_{\mathcal{SR}}\right)^{\alpha}\mathcal{Y}\,\mathrm{EIRP}_{\max}\mathcal{G}_1\left(\rho_{2,B}\right)\mathcal{G}_2\left(\rho_{2,B}\right)}{\left(1-\rho_{ET}^*\right)\eta_{\mathcal{S}}\,a_{\mathcal{RS}}P_{\mathcal{R}}G_{\mathcal{R}}G_{\mathcal{S}}^2} \tag{22}$$

where $\mathcal{G}_1\left(\rho_{2,B}\right)$ and $\mathcal{G}_2\left(\rho_{2,B}\right)$ are obtained by substituting $\rho_2=\rho_{2,B}$ in (20a) and (20b). The positivity of μ_B for $\rho_2^*=\rho_{2,B}$ can be observed from the fact that τ is pseudoconcave in ρ_2 with the single critical point $\rho_{2,C}$ being smaller than $\rho_{2,B}$ in this case. So, global-optimal solution $\boldsymbol{\rho^*}$ for TMP-TA is:

$$(\rho_2^*,\mu^*)=\begin{cases}\left(\rho_{2,B},\mu_B\right), & \rho_{2,C}<\rho_{2,B}\\ \left(\rho_{2,C},0\right), & \rho_{2,B}\leq\rho_{2,C}\\ \text{Infeasible}, & \rho_{ET}^*>1\end{cases} \tag{23}$$

with ρ_0^*,ρ_1^*, and ρ_3^* obtained using ρ_2^* in (15), (17), and (16). Here, $(\boldsymbol{\rho^*},\boldsymbol{\mu^*})$ is also KKT point of TMP-TA. Infeasibility condition $\rho_{ET}^*>1$ implies that the energy demands of $\mathcal{S}$ and/or $\mathcal{D}$ cannot be met by optimized TA with fixed RP because the normalized (per slot period of T s) energy requirement rate $\zeta_{E\mathcal{S}}$ and $\zeta_{E\mathcal{D}}$ of the system is more than optimal RF-EH rate.

B. Optimal Position of i²RES to Maximize τ for a Fixed TA

Now we consider another practical setting where $\mathcal{R}$ (i²RES) is a mobile (or movable) PB with DF relaying capability. In such a setting, to analyze the effect of RP on τ, we optimize the RP for a fixed TA $\boldsymbol{\rho}=\{\rho_0,\rho_1,\rho_2,\rho_3\}$. Investigation on optimal RP is not only important from relay deployment perspective, but it also gives insights on the relay selection policy. It can be noted from (12) and (13), τ is a decreasing function of $d_{\mathcal{SR}}$ and $d_{\mathcal{RD}}$. So, to maximize τ by optimizing RP, $C8$ in TMP should be satisfied at strict equality, i.e., $d_{\mathcal{RD}}=D+\delta-d_{\mathcal{SR}}$. Using this, an equivalent univariate TMP with fixed TA, denoted by TMP-RP, is defined below:

$$\begin{aligned}&\textbf{TMP-RP}:\ \underset{d_{\mathcal{SR}}}{\text{maximize}}\quad\tau,\qquad\text{subject to:}\\ &C1,C2,C3,C6,\qquad C12:d_{\mathcal{SR}}\leq D+\delta-d_{\min}.\end{aligned} \tag{24}$$

In (24), $C12$ is obtained by substituting $d_{\mathcal{RD}}=D+\delta-d_{\mathcal{SR}}$ in $C7$ of TMP. Interestingly, $C2,C3,C6$ provide lower bound d_{LB} on $d_{\mathcal{SR}}$, and $C1,C12$ provide upper bound d_{UB}. These implicit boundary constraints in TMP-RP are defined below:

$$d_{\text{LB}}\triangleq\max\left\{d_{\min},\max\left\{\left(\frac{\rho_1\eta_{\mathcal{S}}\,a_{\mathcal{RS}}P_{\mathcal{R}}G_{\mathcal{R}}G_{\mathcal{S}}^2}{\rho_2\mathcal{Y}\,\mathrm{EIRP}_{\max}}\right)^{\frac{1}{\alpha}},\right.\right.$$
$$\left.\left.D+\delta-\left(\frac{\rho_3\eta_{\mathcal{D}}\,a_{\mathcal{RD}}P_{\mathcal{R}}G_{\mathcal{R}}G_{\mathcal{D}}}{\zeta_{E\mathcal{D}}}\right)^{\frac{1}{\alpha}}\right\}\right\}, \tag{25a}$$

$$d_{\text{UB}}\triangleq\min\left\{\left(\frac{\rho_0\eta_{\mathcal{S}}\,a_{\mathcal{RS}}P_{\mathcal{R}}G_{\mathcal{R}}G_{\mathcal{S}}}{\zeta_{E\mathcal{S}}}\right)^{\frac{1}{\alpha}},D+\delta-d_{\min}\right\}. \tag{25b}$$

With these boundary constraints $d_{\text{LB}}\leq d_{\mathcal{SR}}\leq d_{\text{UB}}$, TMP-RP reduces to an unconstrained problem, with constant bounds on the variable, whose generalized-convexity is proved below.

Theorem 2: The objective function τ in TMP-RP is a pseudoconcave function of $d_{\mathcal{SR}}$ and the equivalent box constraints $d_{\text{LB}}\leq d_{\mathcal{SR}}$ and $d_{\mathcal{SR}}\leq d_{\text{UB}}$ are affine functions of $d_{\mathcal{SR}}$.

Proof: See Appendix B. ∎

Following Theorem 2 and [36, Theorem 4.3.8], optimal RP $d_{\mathcal{SR}}^*$ is given by the KKT point. With υ_1 and υ_2 as Lagrange multipliers for the box constraints, Lagrangian function for TMP-RP is: $\mathcal{L}_d=\tau-\upsilon_1\left[d_{\text{LB}}-d_{\mathcal{SR}}\right]-\upsilon_2\left[d_{\mathcal{SR}}-d_{\text{UB}}\right]$. The three KKT conditions for TMP-RP, apart from the box constraints and non-negativity of υ_1,υ_2, are:

$$\begin{aligned}&\alpha\mathcal{B}R\overline{\mathcal{C}_1}d_{\mathcal{SR}}^{\mathcal{B}\alpha}e^{-\overline{\mathcal{C}_2}\left(D+\delta-d_{\mathcal{SR}}\right)^{\mathcal{B}\alpha}}\left[\overline{\mathcal{C}_2}(D+\delta-d_{\mathcal{SR}})^{\mathcal{B}\alpha-1}\right.\\ &\left.\times\,\mathbf{K_1}\left(\overline{\mathcal{C}_1}d_{\mathcal{SR}}^{\mathcal{B}\alpha}\right)-\overline{\mathcal{C}_1}d_{\mathcal{SR}}^{\mathcal{B}\alpha-1}\mathbf{K_0}\left(\overline{\mathcal{C}_1}d_{\mathcal{SR}}^{\mathcal{B}\alpha}\right)\right]+\upsilon_1=\upsilon_2,\end{aligned} \tag{26a}$$

$$\upsilon_1\left[d_{\text{LB}}-d_{\mathcal{SR}}\right]=0,\qquad\upsilon_2\left[d_{\mathcal{SR}}-d_{\text{UB}}\right]=0 \tag{26b}$$

where $\overline{\mathcal{C}_1}\triangleq\mathcal{C}_1\left(\frac{\rho_2}{\rho_1}\left(2^{\frac{R}{\rho_2}}-1\right)\right)^{\frac{\mathcal{B}}{2}}$ and $\overline{\mathcal{C}_2}\triangleq\mathcal{C}_2\left(2^{\frac{R}{\rho_2}}-1\right)^{\mathcal{B}}$. From Theorem 2 it can be observed that due to pseudoconcavity of τ in $d_{\mathcal{SR}}$ for a fixed TA, τ is given by the feasible critical point $d_{\text{LB}}\leq d_C\leq d_{\text{UB}}$, where the gradient of τ with respect to $d_{\mathcal{SR}}$ vanishes, i.e., $\frac{\partial\tau(d_C)}{\partial d_{\mathcal{SR}}}=0$. Simplified d_C is:

$$d_C\triangleq\left\{d_{\mathcal{SR}}\;\middle|\;1+\left(\frac{\overline{\mathcal{C}_1}\,\mathbf{K_0}\left(\overline{\mathcal{C}_1}d_{\mathcal{SR}}^{\mathcal{B}\alpha}\right)}{\overline{\mathcal{C}_2}\,\mathbf{K_1}\left(\overline{\mathcal{C}_1}d_{\mathcal{SR}}^{\mathcal{B}\alpha}\right)}\right)^{\frac{1}{\mathcal{B}\alpha-1}}=\frac{D+\delta}{d_{\mathcal{SR}}}\right\}. \tag{27}$$

So from (26a), for $d_{\mathcal{SR}}^*=d_C$, $\upsilon_1^*=\upsilon_2^*=0$. However if $d_C<d_{\text{LB}}$, then $d_{\mathcal{SR}}^*=d_{\text{LB}},\upsilon_1^*=-\frac{\partial\tau(d_{\text{LB}})}{\partial d_{\mathcal{SR}}},\upsilon_2^*=0$. Here $\frac{\partial\tau}{\partial d_{\mathcal{SR}}}$ is obtained using (26a) and $\frac{\partial\mathcal{L}_d}{\partial d_{\mathcal{SR}}}=\frac{\partial\tau}{\partial d_{\mathcal{SR}}}+\upsilon_1-\upsilon_2$. Whereas for $d_C>d_{\text{UB}}$, $d_{\mathcal{SR}}^*=d_{\text{UB}},\upsilon_1^*=0,\upsilon_2^*=\frac{\partial\tau(d_{\text{UB}})}{\partial d_{\mathcal{SR}}}$. Also, due to the existence of single critical point d_C because of pseudoconcavity of τ in $d_{\mathcal{SR}}$ (see Theorem 2), $\frac{\partial\tau\left(d_{\mathcal{SR}}^*\right)}{\partial d_{\mathcal{SR}}}=\begin{cases}<0, & \text{if } d_{\text{LB}}>d_C\\ >0, & \text{if } d_{\text{UB}}<d_C\end{cases}$. This proves the non-negativity of the Lagrange multipliers υ_1,υ_2. Thus, leaving trivial case of $d_{\text{LB}}=d_{\text{UB}}$, where the feasible RP region reduces to a single location, the optimal RP $\boldsymbol{d}=\left\{d_{\mathcal{SR}}^*,\ d_{\mathcal{RD}}^*=D+\delta-d_{\mathcal{SR}}^*\right\}$ is given by KKT point $(d_{\mathcal{SR}}^*,\upsilon_1^*,\upsilon_2^*)$ for TMP-RP, defined below:

$$(d_{\mathcal{SR}}^*,\upsilon_1^*,\upsilon_2^*)=\begin{cases}(d_C,0,0), & d_{\text{LB}}\leq d_C\leq d_{\text{UB}}\\ \left(d_{\text{LB}},\frac{-\partial\tau(d_{\text{LB}})}{\partial d_{\mathcal{SR}}},0\right), & d_C<d_{\text{LB}}\leq d_{\text{UB}}\\ \left(d_{\text{UB}},0,\frac{\partial\tau(d_{\text{UB}})}{\partial d_{\mathcal{SR}}}\right), & d_{\text{LB}}\leq d_{\text{UB}}<d_C\\ \text{Infeasible}, & d_{\text{LB}}>d_{\text{UB}}\vee d_x<d_{\min},\end{cases} \tag{28}$$

where $d_x\triangleq\left(G_{\mathcal{R}}P_{\mathcal{R}}\min\left\{\frac{\rho_0\eta_{\mathcal{S}}\,a_{\mathcal{RS}}G_{\mathcal{S}}}{\zeta_{E\mathcal{S}}},\frac{\rho_3\eta_{\mathcal{D}}\,a_{\mathcal{RD}}G_{\mathcal{D}}}{\zeta_{E\mathcal{D}}}\right\}\right)^{\frac{1}{\alpha}}$. Infeasibility condition here implies that optimal RP cannot meet energy demands of $\mathcal{S}$ or $\mathcal{D}$ ($C1$–$C2$), even with $\mathcal{R}$ placed at closest position ($d_{\min}$ or $D+\delta-d_{\min}$) for efficient RF-ET.

C. Joint Optimization of TA and RP to Maximize Throughput

Here, we consider the practical setting with highest degree of freedom, where i^{2}RES has full adaptability in terms of optimizing TA for RF-ET/WIT as well as its relative position between $\mathcal{S}$ and $\mathcal{D}$. Following the univariate formulations TMP-TA and TMP-RP in Sections IV-A and IV-B, the bivariate $(\rho_2, d_{\mathcal{SR}})$ TMP in this case, denoted by TMP-J, is given by:

$$\textbf{TMP-J}: \underset{\rho_2, d_{\mathcal{SR}}}{\text{maximize}} \quad \tau, \qquad \text{subject to:}$$
$$C6, C10, C11, C12, \quad C13: \frac{\widehat{\rho_1}\eta_{\mathcal{S}} a_{\mathcal{RS}} P_{\mathcal{R}} G_{\mathcal{R}} G_{\mathcal{S}}^2}{\rho_2 \left(d_{\mathcal{SR}}\right)^{\alpha} \mathcal{Y}\, \text{EIRP}_{\max}} \leq 1, \tag{29}$$

where $\widehat{\rho_1}$, obtained by using $d_{\mathcal{RD}} = D + \delta - d_{\mathcal{SR}}$ in (17), is:

$$\widehat{\rho_1} \triangleq 1 - 2\rho_2 - \frac{\zeta_{E\mathcal{S}} \left(d_{\mathcal{SR}}\right)^{\alpha}}{\eta_{\mathcal{S}} a_{\mathcal{RS}} P_{\mathcal{R}} G_{\mathcal{R}} G_{\mathcal{S}}} - \frac{\zeta_{E\mathcal{D}} \left(D + \delta - d_{\mathcal{SR}}\right)^{\alpha}}{\eta_{\mathcal{D}} a_{\mathcal{RD}} G_{\mathcal{R}} G_{\mathcal{D}} P_{\mathcal{R}}} \tag{30}$$

and objective τ, which is a function of $\rho_2, d_{\mathcal{SR}}$ only, is obtained by substituting $\rho_1 = \widehat{\rho_1}$ and $d_{\mathcal{RD}} = D + \delta - d_{\mathcal{SR}}$ in (12). Below we prove the joint-pseudoconcavity of τ in ρ_2 and $d_{\mathcal{SR}}$.

Theorem 3: The objective function τ in TMP-J is a jointly pseudoconcave function of ρ_2 and $d_{\mathcal{SR}}$ over the feasible region defined by the constraints $C6, C10$–$C13$.

Proof: See Appendix C. ∎

As noted in Section IV-A, $C10$ and $C11$ are never satisfied at strict equality, i.e., $0 < \rho_2 < \frac{1}{2}$, so they can be considered implicitly. Similarly on considering the box constraints $C6$ and $C12$ on $d_{\mathcal{SR}}$ implicitly along with $C13$ that provides lower bound on $d_{\mathcal{SR}}$ for a given ρ_2, the Lagrangian function for TMP-J is given by objective τ itself. Following Theorem 3, it can be noted that due to the joint-pseudoconcavity of τ, joint-optimal TA and RP are given by the critical point $\left(\rho_{2,JC}, d_{JC}\right)$ (if it exists in the feasible region), which is defined below:

$$\left(\rho_{2,JC}, d_{JC}\right) \triangleq \left\{ \left(\rho_2, d_{\mathcal{SR}}\right) \;\middle|\; \left(\mathcal{G}_2 = 0\right) \wedge \left[\left(\frac{D+\delta}{d_{\mathcal{SR}}} - 1\right)^{\mathcal{B}\alpha - 1} \right.\right.$$
$$\left.\left. = \frac{\left(\widehat{\rho_1} + 1 - \rho_2 - \frac{\zeta_{E\mathcal{D}}\, D \left(D+\delta-d_{\mathcal{SR}}\right)^{\alpha-1}}{\eta_{\mathcal{D}}\, a_{\mathcal{RD}}\, G_{\mathcal{R}}\, G_{\mathcal{D}}\, P_{\mathcal{R}}}\right) \overline{\mathcal{C}_1}\, \mathbf{K_0}\left(\overline{\mathcal{C}_1} d_{\mathcal{SR}}^{\mathcal{B}\alpha}\right)}{2 \left(\widehat{\rho_1}\right)^{1+\frac{\mathcal{B}}{2}} \overline{\mathcal{C}_2}\, \mathbf{K_1}\left(\overline{\mathcal{C}_1} d_{\mathcal{SR}}^{\mathcal{B}\alpha}\right)} \right] \right\}. \tag{31}$$

Actually (31) represents a system of two nonlinear equations to be solved for ρ_2 and $d_{\mathcal{SR}}$. As $0 < \rho_{2,JC} < \frac{1}{2}$, depending on the feasibility of d_{JC} over the constraints $C6$, $C10$ to $C13$, joint-global-optimal TA and RP $(\boldsymbol{\rho^*}, \boldsymbol{d^*})$ that maximizes τ is: $\rho_2^* = \rho_{2,JC}$ and $d_{\mathcal{SR}}^* = \max\left\{d_{\min}, \left(\frac{\widehat{\rho_1}\eta_{\mathcal{S}} a_{\mathcal{RS}} P_{\mathcal{R}} G_{\mathcal{R}} G_{\mathcal{S}}^2}{\rho_{2,JC}\, \mathcal{Y}\, \text{EIRP}_{\max}}\right)^{\frac{1}{\alpha}}, \min\left\{d_{JC}, D + \delta - d_{\min}\right\}\right\}$ with $d_{\mathcal{RD}}^* = D + \delta - d_{\mathcal{SR}}^*$ and $\rho_0^*, \rho_1^*, \rho_3^*$ obtained by substituting $\rho_2^*, d_{\mathcal{SR}}^*, d_{\mathcal{RD}}^*$ in (15), (17), (16). The infeasibility of TMP-J, implying that energy demands cannot be even met by jointly optimized TA-RP, is: $\frac{\zeta_{E\mathcal{S}} \left(d_{\mathcal{SR}}^*\right)^{\alpha}}{\eta_{\mathcal{S}} a_{\mathcal{RS}} P_{\mathcal{R}} G_{\mathcal{R}} G_{\mathcal{S}}} + \frac{\zeta_{E\mathcal{D}} \left(d_{\mathcal{RD}}^*\right)^{\alpha}}{\eta_{\mathcal{D}} a_{\mathcal{RD}} G_{\mathcal{R}} G_{\mathcal{D}} P_{\mathcal{R}}} > 1$. This relationship also provides the upper-bound on the energy demands $\zeta_{E\mathcal{S}}$ and $\zeta_{E\mathcal{D}}$ that can be simultaneously met.

V. Approximation for Global-Optimal TA and RP

In previous section we obtained global-optimal TA and RP solutions for non-convex TMP by exploiting its generalized-convexity. However, the global-optimal solutions for TMP in Section IV are semi-analytical, i.e., the feasible critical points $\rho_{2,C}$ and d_C are obtained numerically and the boundary points (if critical point is infeasible) $\rho_{2,B}$ and $d_{\text{LB}}, d_{\text{UB}}$ are given in closed-form. So, in order to gain further insights, we derive tight analytical approximations for numerical global-optimal TA and RP. This will help in better understanding of the impact of various communication system and RF-EH hardware parameters on the achievable throughput performance.

A. Tight Closed-form Approximation for Optimal TA

To obtain analytical approximation for optimal TA $\rho_2^* = \rho_{2,C}$ in TMP-TA using (20b), the equation $\mathcal{G}_2\left(\rho_2\right) = 0$, when solved numerically for $\rho_2 = \rho_{2,C}$, can be simplified as:

$$\frac{\rho_2\left(1-\rho_{ET}^*\right)\left(2^{\frac{R}{\rho_2}}-1\right) - 2^{\frac{R}{\rho_2}} R \ln(2)\left(1-\rho_{ET}^*-2\rho_2\right)}{2^{\frac{R}{\rho_2}+1}\left(2^{\frac{R}{\rho_2}}-1\right)^{\mathcal{B}} R \ln(2)\left(1-\rho_{ET}^*-2\rho_2\right)\mathcal{C}_2\left(d_{\mathcal{RD}}\right)^{\mathcal{B}\alpha}} = \frac{\mathbf{K_1}(\mathcal{Z})}{\mathcal{Z}\,\mathbf{K_0}(\mathcal{Z})} \tag{32}$$

with $\mathcal{Z} \triangleq \mathcal{C}_1 d_{\mathcal{SR}}^{\mathcal{B}\alpha}\left(\frac{\rho_2}{\rho_1}\left(2^{\frac{R}{\rho_2}}-1\right)\right)^{\frac{\mathcal{B}}{2}}$. Considering practical RF-ET process in WPCN and SWIPT, LoS component can be very strong with $K \gg 1$, which results in high $\mathcal{B}$. This along with $\alpha \geq 2$ and $R \geq 1$ results in very high $\mathcal{Z}$. Thus, on using a limiting property: $\lim_{\mathcal{Z}\to\infty} \frac{\mathbf{K_1}(\mathcal{Z})}{\mathcal{Z}\,\mathbf{K_0}(\mathcal{Z})} = 0$ in (32), we obtain: $\rho_2\left(1-\rho_{ET}^*\right)\left(2^{\frac{R}{\rho_2}}-1\right) = 2^{\frac{R}{\rho_2}} R \ln(2)\left(1-\rho_{ET}^*-2\rho_2\right)$, which after rearrangement reduces to: $2^{\frac{R}{\rho_2}}\left(\frac{R}{\rho_2}\ln\left(\frac{1}{2}\right) + 1 + \frac{R\ln(4)}{1-\rho_{ET}^*}\right) = 1$. On solving this for ρ_2, by using a property that solution for $2^x(ax+b) = c$ is given by $x = \frac{\mathbf{W}\left(\ln(2)\frac{c}{a}2^{\frac{b}{a}}\right)}{\ln(2)} - \frac{b}{a}$, we finally obtain the approximation $\widehat{\rho_{2,C}} \approx \rho_{2,C}$ as:

$$\widehat{\rho_{2,C}} \triangleq \frac{\left(1-\rho_{ET}^*\right)}{2 + \frac{\left(1-\rho_{ET}^*\right)}{R\ln(2)}\left[\mathbf{W}\left(-4^{-\frac{R}{1-\rho_{ET}^*}}\; e^{-1}\right) + 1\right]} \tag{33}$$

where $\rho_{ET}^* = \frac{\zeta_{E\mathcal{S}}\left(d_{\mathcal{SR}}\right)^{\alpha}}{\eta_{\mathcal{S}} a_{\mathcal{RS}} P_{\mathcal{R}} G_{\mathcal{R}} G_{\mathcal{S}}} + \frac{\zeta_{E\mathcal{D}}\left(d_{\mathcal{RD}}\right)^{\alpha}}{\eta_{\mathcal{D}} a_{\mathcal{RD}} G_{\mathcal{R}} G_{\mathcal{D}} P_{\mathcal{R}}}$ and $\mathbf{W}\left(\cdot\right)$ is the Lambert function [37]. (33) provides insights on the interplay between system parameters R, ρ_{ET}^*, and optimal TA $\widehat{\rho_{2,C}}$. The accuracy of this analytical approximation $\widehat{\rho_{2,C}}$ is numerically validated in Section VI-D.

Remark 1: Optimal TA $\widehat{\rho_{2,C}}$ is proportional to threshold rate requirement R and TA $\left(1-\rho_{ET}^*\right)$ other than allocated for energy replenishment of $\mathcal{S}$ and $\mathcal{D}$, which depends on RP.

B. Tight Closed-form Approximation for Optimal RP

Now we obtain tight analytical approximation for d_C defined in (27). After some rearrangement, (27) that needs to be solved for the feasible critical point $d_{\mathcal{SR}} = d_C$ reduces to:

$$\overline{\mathcal{C}_1}\left(d_{\mathcal{SR}}\right)^{\mathcal{B}\alpha-1}\mathbf{K_0}\left(\mathcal{Z}\right) = \overline{\mathcal{C}_2}\left(D+\delta-d_{\mathcal{SR}}\right)^{\mathcal{B}\alpha-1}\mathbf{K_1}\left(\mathcal{Z}\right). \tag{34}$$

Additionally, with the fact that $\alpha \geq 2$, $R \geq 1$ and $K \gg 1$ in WPCN and SWIPT systems, we consider another limiting property of $\mathbf{K_n}\left(\cdot\right)$, stating: $\lim_{\mathcal{Z}\to\infty} \frac{\mathbf{K_1}(\mathcal{Z})}{\mathbf{K_0}(\mathcal{Z})} = 1$. Using this property in (34) and solving for $d_{\mathcal{SR}}$, a tight analytical approximation $\widehat{d_C}$ for $\overline{\mathcal{C}_1} d_{\mathcal{SR}}^{\mathcal{B}\alpha} \gg 1$, is obtained as:

$$d_C \approx \widehat{d_C} \triangleq \frac{\left(D+\delta\right)\left(\overline{\mathcal{C}_2}\right)^{\frac{1}{\mathcal{B}\alpha-1}}}{\left(\overline{\mathcal{C}_1}\right)^{\frac{1}{\mathcal{B}\alpha-1}} + \left(\overline{\mathcal{C}_2}\right)^{\frac{1}{\mathcal{B}\alpha-1}}}. \tag{35}$$

This approximation helps in gaining insights on the impact of various system parameters $P_{\mathcal{R}}, \sigma^2, \eta_{\mathcal{S}}, a_{\mathcal{RS}}, a_{\mathcal{SR}}, a_{\mathcal{RD}}, G_{\mathcal{S}}$, $G_{\mathcal{R}}, G_{\mathcal{D}}, K, \alpha, R$, and $\boldsymbol{\rho}$ on approximated global-optimal RP solution $\widehat{d_C}$. Here we also notice that $\overline{\mathcal{C}_2}$ is inversely proportional to the average SNR of $\mathcal{R}$-to-$\mathcal{D}$ link, and is relatively very small in comparison to $\overline{\mathcal{C}_1}$ because $\mathcal{S}$-to-$\mathcal{R}$ link suffers from doubly-near-far problem. However, optimal RP resolves this problem by placing $\mathcal{R}$ close to $\mathcal{S}$ (cf. Section VI-C2).

Remark 2: Optimal RP $\widehat{d_C}$ is such that $\mathcal{R}$ is placed closer to $\mathcal{S}$ if effective $\mathcal{S}$-to-$\mathcal{R}$ link is poorer than $\mathcal{R}$-to-$\mathcal{D}$ link, i.e., $\overline{\mathcal{C}_2} < \overline{\mathcal{C}_1}$. Otherwise if $\overline{\mathcal{C}_2} > \overline{\mathcal{C}_1}$, $\mathcal{R}$ is placed closer to $\mathcal{D}$.

C. Alternating Optimization based Approximation for TMP-J

Using analytical approximations for $\rho_{2,C}$ and d_C, a two-step alternating optimization scheme Algorithm 1 is presented to obtain tight approximation for joint-optimal TA-RP in TMP-J.

Algorithm 1 starts with an initial RP ($d_{\mathcal{SR}} = d_0, d_{\mathcal{RD}} = D+\delta-d_0$), which is motivated by the fact that maximum τ in TMP-J is obtained by allocating minimum time ρ^*_{ET} for RF-ET to $\mathcal{S}$ and $\mathcal{D}$. Mathematically, $d_0 \triangleq \left\{ d_{\mathcal{SR}} \;\middle|\; \underset{d_{\mathcal{SR}}}{\text{minimize}}\; \rho^*_{ET} \right\} = \left\{ d_{\mathcal{SR}} \;\middle|\; \frac{\partial(\rho^*_0+\rho^*_3)}{\partial d_{\mathcal{SR}}} = 0 \right\} = \frac{D\mathcal{H}_2^{\frac{1}{\alpha-1}}}{\mathcal{H}_1^{\frac{1}{\alpha-1}}+\mathcal{H}_2^{\frac{1}{\alpha-1}}}$, where $\mathcal{H}_1 \triangleq \frac{\zeta_{E\mathcal{S}}}{\eta_{\mathcal{S}} a_{\mathcal{RS}} P_{\mathcal{R}} G_{\mathcal{R}} G_{\mathcal{S}}}$ and $\mathcal{H}_2 \triangleq \frac{\zeta_{E\mathcal{D}}}{\eta_{\mathcal{D}} a_{\mathcal{RD}} G_{\mathcal{R}} G_{\mathcal{D}} P_{\mathcal{R}}}$. For this RP d_0, we iteratively obtain the approximated optimal TA for fixed RP using (23), (33), (15), (17), (16); and optimal RP for just obtained approximated TA using (28) and (35). After two cycles of TMP-TA and TMP-RP each, as also shown in Section VI-D, the obtained approximations for TA and RP closely match with jointly-optimized TA and RP in TMP-J due to its joint-pseudoconcavity (see Theorem 3). Algorithm 1 terminates with a feasible TA $\left(\widehat{\rho^*_0}, \widehat{\rho^*_1}, \widehat{\rho^*_2}, \widehat{\rho^*_3}\right)$ and RP $\left(\widehat{d^*_{\mathcal{SR}}}, \widehat{d^*_{\mathcal{RD}}}\right)$ (feasibility conditions are discussed in Section IV-C) that maximizes τ in TMP-J.

Algorithm 1 Two-step analytical alternating optimization scheme for joint-optimal TA and RP.

Input: $\boldsymbol{d_0} = \left\{ d_{\mathcal{SR},0} = d_0, d_{\mathcal{R},\mathcal{D},0} = D+\delta-d_0 \right\}$
Output: $\widehat{\tau^*}, \widehat{\rho^*_0}, \widehat{\rho^*_1}, \widehat{\rho^*_2}, \widehat{\rho^*_3}, \widehat{d^*_{\mathcal{SR}}}, \widehat{d^*_{\mathcal{RD}}}$

1: Set $i \leftarrow 0$
2: **repeat** (Main Two-step Loop)
3: Set $i \leftarrow i+1$
4: Obtain analytical approximation for optimal TA $\boldsymbol{\rho_i} = \{\rho_{0,i}, \rho_{1,i}, \rho_{2,i}, \rho_{3,i}\}$ for fixed RP $\boldsymbol{d_{i-1}}$ using (23) and (33)
5: Obtain analytical approximation for optimal RP $\boldsymbol{d_i} = \left\{ d_{\mathcal{SR},i}, D+\delta-d_{\mathcal{SR},i} \right\}$ for fixed TA $\boldsymbol{\rho_i}$ using (28) and (35)
6: **until** $(i \geq 2)$ ▷ Two-step means two alternating cycles
7: $d^{\text{arr}}_{\mathcal{SR}} \triangleq \left\{ d_{\min}, \left(\frac{\widehat{\rho_{1,2}} \eta_{\mathcal{S}} a_{\mathcal{RS}} P_{\mathcal{R}} G_{\mathcal{R}} G_{\mathcal{S}}^2}{\rho_{2,2} \mathcal{Y}\, \text{EIRP}_{\max}} \right)^{\frac{1}{\alpha}}, d_{\mathcal{SR},2}, D+\delta-d_{\min} \right\}$
8: Obtain approximated optimal TA $\boldsymbol{\rho}^{\text{arr}} = \{\boldsymbol{\rho}^{\text{arr}}_1, \boldsymbol{\rho}^{\text{arr}}_2, \boldsymbol{\rho}^{\text{arr}}_3, \boldsymbol{\rho}^{\text{arr}}_4\}$ for fixed RP $d^{\text{arr}}_{\mathcal{SR}}$ using (23) and (33)
9: Obtain $\tau^{\text{arr}} = \{\tau^{\text{arr}}_1, \tau^{\text{arr}}_2, \tau^{\text{arr}}_3, \tau^{\text{arr}}_4\}$ by using (13) for each feasible element (maximum four) in $\boldsymbol{\rho}^{\text{arr}}$ and $d^{\text{arr}}_{\mathcal{SR}}$
10: Set $j^* \leftarrow \underset{1\leq j\leq 4}{\text{argmax}} \left\{\tau^{\text{arr}}_j\right\}$ and Set $\widehat{\tau^*} \leftarrow \tau^{\text{arr}}_{j^*}$
11: $\left\{ \widehat{\rho^*_0}, \widehat{\rho^*_1}, \widehat{\rho^*_2}, \widehat{\rho^*_3}, \widehat{d^*_{\mathcal{SR}}}, \widehat{d^*_{\mathcal{RD}}} \right\} \triangleq \left\{ \boldsymbol{\rho}^{\text{arr}}_{j^*}, d^{\text{arr}}_{\mathcal{SR},j^*}, D+\delta-d^{\text{arr}}_{\mathcal{SR},j^*} \right\}$.

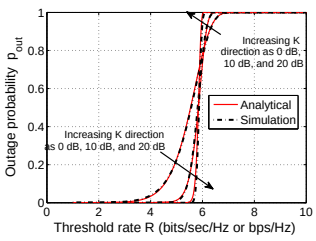

Fig. 4. Validation of outage analysis.

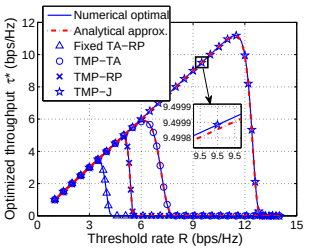

Fig. 5. Variation of τ^* with R.

VI. Performance Evaluation and Validation

We now numerically investigate performance of TMP along with accuracy of analysis under practical constraints. Unless mentioned, below-stated parameters are used for simulations.

Due to a maximum allowable EIRP of $P_{\mathcal{R}} G_{\mathcal{R}} = 4$W, we consider $P_{\mathcal{R}} = 0.4$W with $G_{\mathcal{R}} = 10$. $\mathcal{S}$ and $\mathcal{D}$ are also equipped with directional antenna having gain $G_{\mathcal{S}} = G_{\mathcal{D}} = 10$. Transmission frequency is 915 MHz and $\eta_{\mathcal{S}} = \eta_{\mathcal{D}} = 0.5$. Accounting for other antenna and channel gains, $a_{\mathcal{RS}} = a_{\mathcal{SR}} = a_{\mathcal{RD}} = 0.068$, which are obtained considering received power 27.19 mW at 1 m distance for EIRP $= 4$W and $\alpha = 2$. With noise power spectral density -174 dBm/Hz, $\sigma^2 = 10^{-13}$ W. To incorporate strong LoS component in RF-ET, $K = 10$. Without the loss of generality, we assume $T = 1$ sec and $\mathcal{R}$ to be located such that $d_{\min} = 0.5$ m and $d_{\mathcal{SR}} + d_{\mathcal{RD}} = D$, i.e., $\delta = 0$. However, position of $\mathcal{R}$ is not necessarily on the line joining $\mathcal{S}$ and $\mathcal{D}$, i.e., $\delta \geq 0$. Feasible range for RP given by D is constrained by limited RF-ET range and low energy sensitivity of around -20 dBm [2]. To ensure that received RF power at $\mathcal{S}$ and $\mathcal{D}$ is more than -20 dBm to enable RF-EH, we found that $D = 52.15$ m for $\alpha = 2$, and $D = 13.96$ m for $\alpha = 3$. We consider $\alpha = 2$ with normalized EH requirements of $\mathcal{S}$ and $\mathcal{D}$ as $\zeta_{E\mathcal{S}} = 10^{-6}$ J/s and $\zeta_{E\mathcal{D}} = 10^{-7}$ J/s. For comparison, we consider fixed TA-RP scheme with $\rho_0 = \rho_3 = 0.02$, $\rho_2 = 0.2$, and $d_{\mathcal{SR}} = \frac{D}{4}$ because $\mathcal{S}$-to-$\mathcal{R}$ link suffers from doubly-near-far problem [9].

A. Validation of Outage Probability Analysis

First, we validate the closed-form outage probability p_{out} expression (12) derived using our proposed exponential fit for $Q_1(a,b)$ with high a. Analytical results for p_{out} in Fig. 4 with varying K and R are obtained using (12) with $\rho_1 = \rho_2 = 0.3$ and $d_{\mathcal{SR}} = 0.2D$. Whereas simulation results are generated by finding p_{out} in 10^7 random realization of Rician fading channel gains $(h_{\mathcal{RS}}, h_{\mathcal{SR}}, h_{\mathcal{RD}})$ with different K. As delay-limited throughput τ in (13) is itself a function of p_{out}, analytical validation of p_{out} also verifies throughput analysis. *Results in Fig. 4, show that analytically-obtained p_{out} closely matches with the simulation results, with a RMSE < 0.022.*

B. Optimized Throughput Performance of Proposed Schemes

Now we discuss the relative performance of TMP-TA, TMP-RP, and TMP-J schemes against benchmark fixed TA-RP scheme. In Figs. 5, 6, and 7, we have plotted the variation of maximum achievable throughput against: (i) transmission or outage threshold rate R, (ii) Rice factor K, and (iii) $\zeta_{E\mathcal{D}}$.

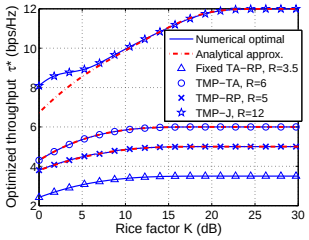

Fig. 6. Variation of τ^* with K.

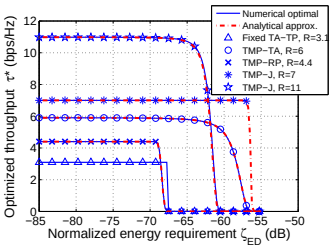

Fig. 7. Variation of τ^* with $\zeta_{E\mathcal{D}}$.

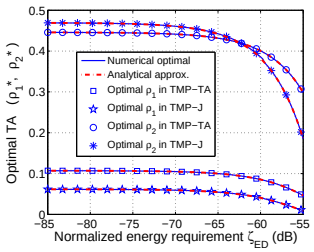

Fig. 8. Variation of ρ_1^* and ρ_2^* in TMP-TA and TMP-J with $\zeta_{E\mathcal{D}}$.

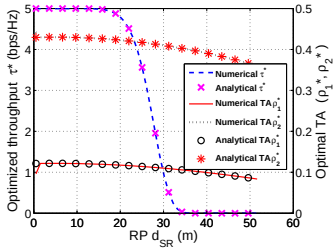

Fig. 9. Variation of τ^*, ρ_1^*, and ρ_2^* in TMP-TA with $d_{\mathcal{SR}}$.

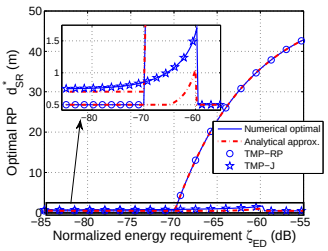

Fig. 10. Variation of $d_{\mathcal{SR}}^*$ in TMP-RP and TMP-J with $\zeta_{E\mathcal{D}}$.

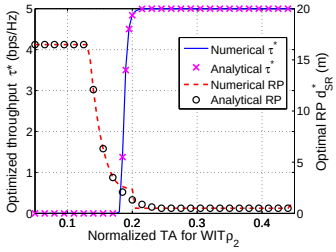

Fig. 11. Variation of τ^* and $d_{\mathcal{SR}}^*$ in TMP-RP with ρ_2.

1) Variation with R: From Fig. 5 we observe that fixed TA-RP scheme fails to provide positive τ for delay-limited systems with $R > 4.4$ bps/Hz. Proposed semi-adaptive schemes TMP-TA and TMP-RP can respectively meet rate requirements of up to 7.7 and 5.7 bps/Hz. Whereas, *joint-optimal TA-RP (TMP-J) can meet much higher rate requirements of up to* 13.1 *bps/Hz.*

2) Variation with K: Fig. 6 shows that the *performance of each scheme improves with increased Rice factor K due to lesser energy loss in wireless dissipation.* The performance improvement of fixed, TMP-RP, and TMP-TA with increased K respectively saturate at 3.5, 5, and 6 bps/Hz. On other hand performance of TMP-J saturates at 12 bps/Hz for $K > 25$ dB.

Remark 3: TMP-TA is a better semi-adaptive scheme as compared to TMP-RP. TMP-J outperforms all schemes and respectively provides about three-times and two-times higher throughput than that achieved by fixed TA-RP and TMP-RP.

3) Variation with $\zeta_{E\mathcal{D}}$: Via Fig. 7, we investigate an inherent tradeoff between optimized rate-constrained throughput and minimum energy requirement at $\mathcal{D}$. As with $T = 1$ sec the units for $\zeta_{E\mathcal{S}}$ and $\zeta_{E\mathcal{D}}$ are J/s or W, we have represented $\zeta_{E\mathcal{D}}$ in dB. On solving this Pareto-optimal tradeoff for each case, we obtain that fixed TA-RP scheme can only sustain energy requirement of up to $\zeta_{E\mathcal{D}} = -67.75$ dB, while providing positive τ for $R = 3.5$ bps/Hz at $\mathcal{D}$. TMP-TA and TMP-RP can respectively meet rate R requirements of up to 6 bps/Hz and 4.4 bps/Hz while providing perpetual operation to $\mathcal{D}$ with average normalized energy requirement of less than -56.5 dB and -67.75 dB. However, TMP-J has capability of providing uninterrupted operation to $\mathcal{D}$ with $\tau > 0$ for $R = 11$ bps/Hz and $R = 7$ bps/Hz while meeting its respective EH requirements of less than -60.5 and -56 dB. This corroborates the importance of jointly-optimizing TA-RP.

Remark 4: SWIPT to $\mathcal{D}$, meeting its energy requirements $\zeta_{E\mathcal{D}}$, influences $\mathcal{R}$-assisted WPCN throughput performance by reducing time $(1-\rho_3)\,T$ available for WIT and RF-ET to $\mathcal{S}$.

C. Insights on Optimal Time Allocation and Relay Placement

1) Optimal TA: In Fig. 8, we plot the variation of optimal TA ρ_1^*, ρ_2^* in TMP-TA and TMP-J with $\zeta_{E\mathcal{D}}$. Results show that ρ_1^* and ρ_2^* decrease with increased $\zeta_{E\mathcal{D}}$ due to increasing share of TA ρ_3^* for energy replenishment of $\mathcal{D}$. TMP-J allocates higher ρ_2^* (time for WIT) than TMP-TA for lower $\zeta_{E\mathcal{D}}$, which is one of the reasons for its improved throughput performance (cf. Fig. 7). The sharper decrease in ρ_2^* for TMP-J than TMP-TA at higher $\zeta_{E\mathcal{D}}$ is due to the need for keeping $\mathcal{R}$ at a favorable location (close to $\mathcal{S}$, see Fig. 10) while meeting $\zeta_{E\mathcal{D}}$.

The variation of optimal throughput τ^* and ρ_1^*, ρ_2^* in TMP-TA with $R = 5$ bps/Hz and varying RP $d_{\mathcal{SR}}$ is plotted in Fig. 9. Results show that $\tau^*, \rho_1^*, \rho_2^*$ in TMP-TA decrease with increased $d_{\mathcal{SR}}$ due to increasing share of TA ρ_0^* for energy replenishment of $\mathcal{S}$ and weakening of $\mathcal{S}$-to-$\mathcal{R}$ link. *No throughput is achieved by TMP-TA if $d_{\mathcal{SR}} > 40$ m and highest is achieved when $\mathcal{R}$ is placed very close to $\mathcal{S}$.*

2) Optimal RP: Results plotted in Fig. 10 show that optimal RP in both TMP-RP and TMP-J increases with increased $\zeta_{E\mathcal{D}}$ for meeting the increasing energy demands of $\mathcal{D}$. However, this leads to poorer throughput performance due to weakening of $\mathcal{S}$-to-$\mathcal{R}$ link. In TMP-J this problem can be resolved to some extent because here higher energy requirement of $\mathcal{D}$ can be met even with lower $d_{\mathcal{SR}}^*$ (cf. Fig. 10) by increasing ρ_3^* (which implies decreasing ρ_2^* as shown in Fig. 8).

We also plot the variation of optimal RP and optimized throughput in TMP-RP with TA ρ_2 (or ρ_1) for $\rho_0 = \rho_3 = 0.02$ and $R = 5$ bps/Hz in Fig. 11. Results show that for very low ρ_2, $\mathcal{R}$-to-$\mathcal{D}$ link is bottleneck, which cannot be improved by moving $\mathcal{R}$ beyond a maximum distance from $\mathcal{S}$, as it will lead to violation of $C1$. Thus, $\tau^* = 0$ for low ρ_2. However as ρ_2 increases $\mathcal{R}$-to-$\mathcal{D}$ link improves due to decreased $\overline{C_2}$ and at the same time weakened $\mathcal{S}$-to-$\mathcal{R}$ link due to decreased ρ_1 can be improved by placing $\mathcal{R}$ close to $\mathcal{S}$ and thus leading to increasing τ^*. However after certain value of ρ_2 close to 0.35, $\mathcal{S}$-to-$\mathcal{R}$ link cannot be further improved and it becomes bottleneck due to lower bound d_{LB} on $d_{\mathcal{SR}}$. For comparison with results shown in Figs. 9 and 11, we note that TMP-J achieves $\tau^* = 10.96$ bps/Hz for $R = 11$ bps/Hz with *optimal TA* $\rho_1^* = 0.0592, \rho_2^* = 0.461$, *and optimal RP* $d_{\mathcal{SR}}^* = 0.853$ *m.*

Remark 5: Higher TA ρ_2 for WIT with sufficiently enough RF-ET time ρ_0, ρ_1, ρ_3, and $\mathcal{R}$ *placed closer to* $\mathcal{S}$ helps in enhancing throughput performance of i^{2}RES-powered SWIPT.

Remark 6: WPCN suffers from *doubly-near-far* problem,

limiting the optimal throughput performance because $\mathcal{S}$-to-$\mathcal{R}$ link becomes bottleneck in comparison to $\mathcal{R}$-to-$\mathcal{D}$ SWIPT. So, the optimal RP is very close to 8, which also corroborates the reasons for considering no direct $\mathcal{S}$-to-$\mathcal{D}$ link and directional antennas for efficient $\mathcal{R}$-assisted WPCN and $\mathcal{R}$-to-$\mathcal{D}$ SWIPT.

D. Validation of Approximation for Optimal TA and RP

Results obtained in Figs. 5, 6, and 7 for optimized throughput using numerical global-optimal solutions given in Section IV and analytical approximated optimal solutions derived in Section V are almost equal, except for TMP-J with $K < 5$ as shown in Fig. 6. Here the limiting case assumptions discussed in Sections V-A and V-B for ratio of modified Bessel functions of second kind, which are valid for $K \gg 1$, do not hold good for TMP-J with $K < 5$ because it involves compounded approximation errors for both TMP-TA and TMP-RP. So approximation errors that are negligible for TMP-TA and TMP-RP, cannot be ignored in TMP-J for $K < 5$.

We have also validated the accuracy of the proposed approximations for global-optimal TA and RP in Figs. 8, 9, 10, and 11. Results in Figs. 8 and 9 show that optimal TA ρ_2^* for TMP-TA and TMP-J obtained numerically and analytically match very closely with negligible difference of respectively less than 8.6×10^{-5} and 1.1×10^{-3}. From Figs. 10 and 11, it is noted that there is a finite average difference of about 0.24 m and 0.26 m between numerical global-optimal RP and its analytical approximation respectively for TMP-RP and TMP-J (cf. zoomed plot in Fig. 10). A slight mismatch between the numerical optimal RP and its analytical approximation is observed in Fig. 11 for $0.18 < \rho_2 < 0.23$, because $\mathcal{Z} < 1$ for $\rho_2 > 0.18$, which degrades the quality of approximation that holds tight for $\mathcal{Z} \gg 1$. However when $\rho_2 \geq 0.23$, both numerical global-optimal RP and its corresponding analytical approximation are given by the corner point d_{LB} and again the tight approximation holds good $\forall \rho_2 \geq 0.23$. Irrespective of this slight difference in analytical approximation of optimal RP, their optimized throughput performance, as potted in Fig. 11, remains almost the same. Overall, the average difference in throughput performance of numerical solution and its analytical approximation is respectively less than 1.6×10^{-11}, 0.0022, and 0.045 for TMP-TA, TMP-RP, and TMP-J.

Remark 7: For high K in SWIPT and WPCN systems [4], [21], the results with the proposed analytical approximation match very closely with both global-maximum τ and global optimal TA-RP. This validates accuracy of the closed-form expressions (33), (35), and Algorithm 1, which are computationally much more efficient and provide analytical insights.

E. Futuristic Significance of the Proposed System Model

We now discuss the significance of our proposed optimized cooperative RF-EH and information relaying system model in the light of RF-EH technology growth, e.g., improvement in RF-to-dc rectification efficiency $\eta = \eta_{\mathcal{S}} = \eta_{\mathcal{D}}$. Fig. 12 shows that for both independent and perfectly correlated $h_{\mathcal{R}\mathcal{S}}$ and $h_{\mathcal{S}\mathcal{R}}$ scenarios the Pareto-optimal rate-energy tradeoff in TMP-J is around 11 bps/Hz while meeting $\zeta_{E\mathcal{S}} = \zeta_{E\mathcal{D}} = -85$ dB with $\eta = 0.5$, which improves to 11.15 bps/Hz with $\eta = 0.7$ and 11.3 bps/Hz with $\eta = 0.9$. This enhancement in throughput is much more significant at a higher energy requirement $\zeta_{E\mathcal{S}} = \zeta_{E\mathcal{D}} = -55$ dB, where optimized throughput in TMP-J increases by 67% with an increased η from 0.5 to 0.9. We also notice that independent channel gains case offers slightly higher τ^* with an average improvement of 0.0365% over that in perfectly correlated case discussed later in Section VII-A.

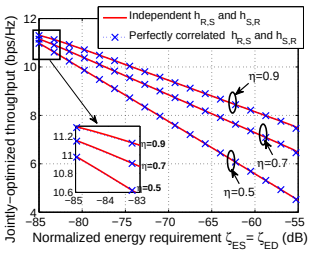

Fig. 12. Improvement in rate-energy tradeoff with increased η.

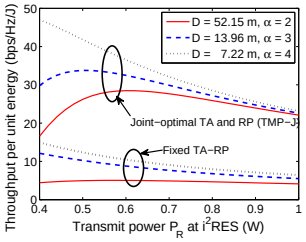

Fig. 13. Energy-efficient throughput performance enhancement.

Lastly, we demonstrate that optimal performance of the proposed relay-powered SWIPT can provide significant improvement in achievable throughput per unit energy consumption at $\mathcal{R}$. As i^{2}RES is the sole energy source in the system model (cf. Fig. 2), which transmits at $P_{\mathcal{R}}$ only during $(1-\rho_2)T$ sec, throughput per unit energy consumed at $\mathcal{R}$, as plotted in Fig. 13, is given by $\frac{\tau}{P_{\mathcal{R}}(1-\rho_2)T}$. From Fig. 13 we note that, decreasing α leads to increasing threshold distance D for receiving atleast -20 dBm RF power from $\mathcal{R}$. The increase in transmit power is considered to incorporate the effect of highly focused beams at $\mathcal{R}$ [1], MIMO technologies [20], or distributed beamforming at $\mathcal{D}$ [2]. Results in Fig. 13 show that, with TMP-J average throughput per unit energy consumption at $\mathcal{R}$ is respectively 5.4, 3.6, and 3.5 times higher than that in fixed TA-RP scheme at varying D as 52.15 m, 13.96 m, and 7.22 m. *Thus, with future advancements in RF-ET technology, the proposed system model for uninterrupted operation of wireless powered devices can lead to an energy-efficient communication with much larger coverage range.*

VII. Discussion and Research Extensions

Now we discuss some potential research extensions of this work. First we note that, the analysis and optimization carried out in this paper can be extended to Nakagami-m fading channels by using the relationship $m = \frac{(K+1)^2}{2K+1}$ between the fading parameter m and Rice factor K [27]. Also, the achievable gains through optimized TA and RP can be further enhanced by considering a multi-antenna i^{2}RES system.

Below, we discuss how the analysis behaves when certain practical system and channel model assumptions are relaxed. Subsequently, we suggest some future research directions.

A. Perfectly Correlated Channel Gains $|h_{\mathcal{R}\mathcal{S}}|^2$ and $|h_{\mathcal{S}\mathcal{R}}|^2$

SNR $\gamma_{\mathcal{S}\mathcal{R}}^{\text{dep}}$ of $\mathcal{S}$-to-$\mathcal{R}$ link under channel reciprocity with $a_{\mathcal{R}\mathcal{S}} = a_{\mathcal{S}\mathcal{R}}$ and perfectly correlated $h_{\mathcal{R}\mathcal{S}}$ and $h_{\mathcal{S}\mathcal{R}}$ reduces to scaled square of the random variable $|h_{\mathcal{S}\mathcal{R}}|^2$. Its CCDF is:

$$\Pr\left[\gamma_{\mathcal{S}\mathcal{R}}^{\text{dep}} > x\right] = e^{-\frac{e_1\left(d_{\mathcal{S}\mathcal{R}}\right)^{\mathcal{B}\alpha}}{2}\left(\frac{\rho_2 x}{\rho_1}\right)^{\frac{\mathcal{B}}{2}}}. \tag{36}$$

Using (10) and (36), the outage probability $p_{out}^{\text{dep}} = \Pr\left(\min\left\{\gamma_{\mathcal{S}\mathcal{R}}^{\text{dep}}, \gamma_{\mathcal{R}\mathcal{D}}\right\} < 2^{\frac{R}{\rho_2}} - 1\right)$ in this case is given by:

$$p_{out}^{\text{dep}} = 1 - e^{-\frac{\mathrm{e}_1 d_{\mathcal{S}\mathcal{R}}^{\mathcal{B}\alpha}}{2}\left(\frac{\rho_2}{\rho_1}\left(2^{\frac{R}{\rho_2}}-1\right)\right)^{\frac{\mathcal{B}}{2}} - \mathrm{e}_2\left(2^{\frac{R}{\rho_2}}-1\right)^{\mathcal{B}} d_{\mathcal{R}\mathcal{D}}^{\mathcal{B}\alpha}}. \quad (37)$$

We notice that (36) and (37) can be respectively obtained from (11) and (12) by replacing $x\,\mathbf{K_1}(x)$ with $e^{-\frac{x}{2}}$. Also, the generalized-convexity results for TMP-TA, TMP-RP, and TMP-J, respectively presented in Theorems 1, 2, and 3, by assuming independence of $h_{\mathcal{R}\mathcal{S}}$ and $h_{\mathcal{S}\mathcal{R}}$, also hold true when they are perfectly correlated (unity correlation coefficient). These results hold because the pseudoconcavity and log-concavity of $\overline{F_{\gamma_{\mathcal{S}\mathcal{R}}}}$ respectively in ρ_2 and $d_{\mathcal{S}\mathcal{R}}$, also hold for $\overline{F_{\gamma_{\mathcal{S}\mathcal{R}}}^{\text{dep}}} = e^{-\frac{\mathrm{e}_1\left(d_{\mathcal{S}\mathcal{R}}\right)^{\mathcal{B}\alpha}}{2}\left(\frac{\rho_2}{\rho_1}\left(2^{\frac{R}{\rho_2}}-1\right)\right)^{\frac{\mathcal{B}}{2}}}$. In fact, the critical point $\widehat{\rho_{2,C}}$, that also provides a tight analytical approximation for $\rho_{2,C}$ in TMP-TA, is same for both $\overline{F_{\gamma_{\mathcal{S}\mathcal{R}}}^{\text{dep}}}$ and $\overline{F_{\gamma_{\mathcal{S}\mathcal{R}}}}$. Furthermore, the tight approximation $\widehat{d_C}$ for d_C in TMP-RP also remains the same irrespective of the two assumptions. Thus, we conclude that the proposed generalized convexity based global-optimization and tight approximation results are valid regardless of the independence of $h_{\mathcal{R}\mathcal{S}}$ and $h_{\mathcal{S}\mathcal{R}}$.

B. Single Omnidirectional Antenna at $\mathcal{R}$ for Energy Broadcast

In this section we show that, irrespective of whether directional or omnidirectional ET from $\mathcal{R}$ is considered, the proposed optimization and analytical solutions are valid. However, with single omnidirectional antenna at $\mathcal{R}$, explicit time slots of duration $\rho_0 T$ and $\rho_3 T$ for RF-ET to $\mathcal{S}$ and $\mathcal{D}$ are not required, because with omnidirectional broadcast of energy from $\mathcal{R}$, $\mathcal{S}$ and $\mathcal{D}$ can respectively harvest energy over $\rho_2 T$ duration of WIT to $\mathcal{D}$ in stage 3 and over $\rho_1 T$ duration of RF-ET to $\mathcal{S}$ in stage 1. The harvested energies $E_{_{\mathcal{S}_0}}$ and $E_{_{\mathcal{D}}}$ at $\mathcal{S}$ and $\mathcal{D}$ for carrying out their respective regular operations get updated as: $E_{_{\mathcal{S}_0}} = \eta_{_{\mathcal{S}}} P_{_{\mathcal{R}}} |h_{_{\mathcal{R}\mathcal{S}}}|^2 \rho_2 T$ and $E_{_{\mathcal{D}}} = \eta_{_{\mathcal{D}}} P_{_{\mathcal{R}}} |h_{_{\mathcal{R}\mathcal{D}}}|^2 \rho_1 T$. Thus, with this omnidirectional ET setting, the optimal $\rho_0^* = \rho_3^* = 0$ (or $\rho_{_{ET}}^* = 0$) and $\rho_1^* = 1 - 2\rho_2^*$. On substituting these values in TMP-TA, we note that the generalized-convexity results proved in Theorem 1 considering two directional antennas at $\mathcal{R}$ also hold for the omnidirectional case. The critical point $\rho_{2,C}^{\text{om}} = \left\{\rho_2 \;\middle|\; \left(\mathcal{G}_2(\rho_2) = 0\right) \wedge \left(\rho_{_{ET}}^* = 0\right)\right\}$ for omnidirectional ET case can be obtained from the critical point $\rho_{2,C}$ defined for directional antenna case by simply substituting $\zeta_{_{E\mathcal{S}}} = 0$ and $\zeta_{_{E\mathcal{D}}} = 0$ to ensure $\rho_0^* = 0$ and $\rho_3^* = 0$, respectively. Similarly, the boundary point $\rho_{2,B}^{\text{om}} = \frac{\eta_{\mathcal{S}} a_{\mathcal{R}\mathcal{S}} P_{\mathcal{R}} G_{\mathcal{R}} G_{\mathcal{S}}^2}{2\eta_{\mathcal{S}} a_{\mathcal{R}\mathcal{S}} P_{\mathcal{R}} G_{\mathcal{R}} G_{\mathcal{S}}^2 + \left(d_{\mathcal{S}\mathcal{R}}\right)^{\alpha} \text{EIRP}_{\max}}$ satisfying $C3$ in this case is obtained from $\rho_{2,B}$ by substituting $\rho_{_{ET}}^* = 0$ in (21). However in case of single omnidirectional antenna, ρ_1^* and ρ_2^* also need to satisfy the energy demands of $\mathcal{D}$ and $\mathcal{S}$ which puts lower bounds on each of them, given by: $\rho_1^* \geq \frac{\zeta_{E\mathcal{D}}\left(d_{\mathcal{R}\mathcal{D}}\right)^{\alpha}}{\eta_{\mathcal{D}} a_{\mathcal{R}\mathcal{D}} G_{\mathcal{R}} G_{\mathcal{D}} P_{\mathcal{R}}}$ and $\rho_2^* \geq \frac{\zeta_{E\mathcal{S}}\left(d_{\mathcal{S}\mathcal{R}}\right)^{\alpha}}{\eta_{\mathcal{S}} a_{\mathcal{R}\mathcal{S}} P_{\mathcal{R}} G_{\mathcal{R}} G_{\mathcal{S}}}$. Using $\rho_1^* = 1 - 2\rho_2^*$, these bounds can be rewritten as: $\frac{\zeta_{E\mathcal{S}}\left(d_{\mathcal{S}\mathcal{R}}\right)^{\alpha}}{\eta_{\mathcal{S}} a_{\mathcal{R}\mathcal{S}} P_{\mathcal{R}} G_{\mathcal{R}} G_{\mathcal{S}}} \leq \rho_2 \leq \frac{1}{2} - \frac{\zeta_{E\mathcal{D}}\left(d_{\mathcal{R}\mathcal{D}}\right)^{\alpha}}{2\eta_{\mathcal{D}} a_{\mathcal{R}\mathcal{D}} G_{\mathcal{R}} G_{\mathcal{D}} P_{\mathcal{R}}}$. Thus, global-optimal solution $\boldsymbol{\rho}^*$ for TMP-TA with omnidirectional RF-ET is: $\rho_2^* = \min\left\{\frac{1}{2} - \frac{\zeta_{E\mathcal{D}}\left(d_{\mathcal{R}\mathcal{D}}\right)^{\alpha}}{2\eta_{\mathcal{D}} a_{\mathcal{R}\mathcal{D}} G_{\mathcal{R}} G_{\mathcal{D}} P_{\mathcal{R}}}, \max\left\{\rho_{2,B}^{\text{om}}, \rho_{2,C}^{\text{om}}, \frac{\zeta_{E\mathcal{S}}\left(d_{\mathcal{S}\mathcal{R}}\right)^{\alpha}}{\eta_{\mathcal{S}} a_{\mathcal{R}\mathcal{S}} P_{\mathcal{R}} G_{\mathcal{R}} G_{\mathcal{S}}}\right\}\right\}$ with $\rho_0^* = \rho_3^* = 0$ and $\rho_1^* = 1 - 2\rho_2^*$. The infeasibility conditions, based on the inability of ρ_2^* (or ρ_1^* as $\rho_1^* = 1 - 2\rho_2^*$) in meeting either of the energy demands $\zeta_{E\mathcal{S}}$ or $\zeta_{E\mathcal{D}}$, are given by the set: $\left(\max\left\{\frac{\zeta_{E\mathcal{S}}\left(d_{\mathcal{S}\mathcal{R}}\right)^{\alpha}}{\eta_{\mathcal{S}} a_{\mathcal{R}\mathcal{S}} P_{\mathcal{R}} G_{\mathcal{R}} G_{\mathcal{S}}}, \frac{\zeta_{E\mathcal{D}}\left(d_{\mathcal{R}\mathcal{D}}\right)^{\alpha}}{2\eta_{\mathcal{D}} a_{\mathcal{R}\mathcal{D}} G_{\mathcal{R}} G_{\mathcal{D}} P_{\mathcal{R}}}\right\} > \frac{1}{2}\right) \vee \left(\frac{\zeta_{E\mathcal{S}}\left(d_{\mathcal{S}\mathcal{R}}\right)^{\alpha}}{\eta_{\mathcal{S}} a_{\mathcal{R}\mathcal{S}} P_{\mathcal{R}} G_{\mathcal{R}} G_{\mathcal{S}}} > \frac{1}{2} - \frac{\zeta_{E\mathcal{D}}\left(d_{\mathcal{R}\mathcal{D}}\right)^{\alpha}}{2\eta_{\mathcal{D}} a_{\mathcal{R}\mathcal{D}} G_{\mathcal{R}} G_{\mathcal{D}} P_{\mathcal{R}}}\right)$.

Similarly, the optimal RP for omnidirectional antenna case can be obtained from (28) with d_C defined in (27), d_{LB} and d_{UB} defined in (25a) and (25b) with ρ_0 and ρ_3 respectively replaced by ρ_2 and ρ_1. Also, the generalized-convexity results for TMP-RP with directional ET in Theorem 2 hold for the omnidirectional antenna case. Finally, the joint optimization results with omnidirectional antenna can be obtained by substituting $\widehat{\rho_1} = 1 - 2\rho_{2,JC}$ and $\zeta_{E\mathcal{S}} = \zeta_{E\mathcal{D}} = 0$ in joint optimal $\left(\rho_2^*, d_{\mathcal{S}\mathcal{R}}^*\right)$, defined for directional antenna case in Section IV-C. The other optimal solutions are obtained as: $d_{\mathcal{R}\mathcal{D}}^* = D + \delta - d_{\mathcal{S}\mathcal{R}}^*$, $\rho_0^* = \rho_3^* = 0, \rho_1^* = 1 - 2\rho_2^*$. The infeasibility conditions are similar to that in TMP-TA, but with optimized RP $\left(d_{\mathcal{S}\mathcal{R}}^*, d_{\mathcal{R}\mathcal{D}}^*\right)$.

Now we compare the optimal throughput τ^* performance of TMP-J for single omnidirectional antenna case with that of two directional antennas at $\mathcal{R}$ (cf. Section IV-C). We observe that, with the same transmit power $P_{_{\mathcal{R}}} = 0.4$ W, the maximum RF-ET range D for $\alpha = 2$ reduces from 52.15 m for the directional antenna case having $G_{_{\mathcal{R}}} = 10$ to 16.49 m with omnidirectional antenna having $G_{_{\mathcal{R}}} = 1$. Further, even if this range constraint is relaxed, we note that TMP-J for omnidirectional antenna case achieves $\tau^* = 4.33$ *bps/Hz, with* $\rho_0^* = \rho_3^* = 0$, $\rho_1^* = 0.0615, \rho_2^* = 0.4692$, *and* $d_{\mathcal{S}\mathcal{R}}^* = 0.5142$ *m*, which is much lower than $\tau^* = 10.96$ bps/Hz achieved with two directional antennas at $\mathcal{R}$ for the parameters considered in Section VI-C.

C. Instantaneous CSI based TMP

In this work we have not considered instantaneous CSI based optimization, which otherwise provides better performance. This is because it incurs significant signaling overhead on battery-constrained EH nodes [19]–[23], [32]. Here we show that, the statistical CSI-based optimization carried out in Sections IV and V not only provides lower bound on the achievable throughput performance, but also gives valuable insights on the instantaneous CSI based optimization.

The instantaneous throughput is given by: $\tau_{\text{ins}} = \rho_2 \log_2(1 + \min\{\gamma_{\mathcal{S}\mathcal{R}}, \gamma_{\mathcal{R}\mathcal{D}}\})$. As $\rho_2 \log_2(1 + \gamma_{\mathcal{S}\mathcal{R}})$ is concave in ρ_2 and $\rho_2 \log_2(1 + \gamma_{\mathcal{R}\mathcal{D}})$ is strictly increasing in ρ_2, it can be easily shown that maximum τ_{ins} is obtained at the ρ_2^* that uniquely maximizes $\rho_2 \log_2(1 + \gamma_{\mathcal{S}\mathcal{R}})$. With this ρ_2^*, optimal RP $d_{\mathcal{S}\mathcal{R}}^*$ is obtained by making the rate over the two links equal, i.e., by solving $\gamma_{\mathcal{S}\mathcal{R}} = \gamma_{\mathcal{R}\mathcal{D}}$. This RP $d_{\mathcal{S}\mathcal{R}}^*$ is unique and gives the joint global-optimal solution along with ρ_2^*. Interestingly, the approximation results $\widehat{\rho_{2,C}}$ and $\widehat{d_C}$ are also based on similar concepts, i.e., TA based on individual optimization of $\overline{F_{\gamma_{\mathcal{S}\mathcal{R}}}}$ and optimally placing $\mathcal{R}$ to ensure $\gamma_{\mathcal{S}\mathcal{R}} \approx \gamma_{\mathcal{R}\mathcal{D}}$.

D. Future Research Directions

1) Energy Accumulation at EH Nodes for Future Use: As we have considered quasi-static block fading assumption

with only statistical CSI availability, $\mathcal{S}$ uses all of its harvested energy $E_{\mathcal{S}_1}$ during $\rho_1 T$ for carrying out WIT over duration $\rho_2 T$. Therefore, without the need of batteries, this helps in realization of low-cost IoT devices connected with relatively cheap passive RF-EH $\mathcal{S}$ and $\mathcal{D}$ that are fully-powered by i^{2}RES. The optimized throughput performance can be further enhanced if instantaneous CSI is available and some part of the harvested energy during $\rho_1 T$ can be spared for *future use*. However, this requires a detailed investigation because the increased gain is achieved at the cost of increased signalling overhead at $\mathcal{S}$ and $\mathcal{D}$ along with increased computational overhead at $\mathcal{R}$ to find optimal TA-RP using an online algorithm.

2) Delay-Tolerant Throughput Maximization: Although an outage based throughput definition has been considered to investigate optimized performance of RF-powered delay-limited cooperative communication, the analysis and optimization results in Sections IV and V provide useful insights on optimal TA and RP in delay-tolerant communication scenario as well, because the optimized solutions follow a similar trend in ergodic capacity based TMP, as shown in [19], [38].

3) Adopting Power Splitting (PS) Scheme at EH Destination: We have preferred time switching (TS) over PS at $\mathcal{D}$ to have single protocol to control all the stages. However, even for PS scheme the optimization formulation and solution methodology is similar to that proposed in Sections III, IV, and V. Interestingly the global-optimal RP solution and its analytical approximation in TMP-RP remain unchanged irrespective of whether PS or TS is employed at $\mathcal{D}$.

VIII. Concluding Remarks

To summarize, we have proposed a novel i^{2}RES-assisted cooperative communication between energy-constrained wireless nodes. Since the LoS signal component can be strong in communications involving RF-ET, in system performance analysis we have considered Rician channel model, where we have proposed a highly accurate exponential approximation. Via closed-form analysis and generalized-convexity proofs, we have captured the optimal system performance under constrained RP (TMP-TA) and constrained TA (TMP-RP), as well as in an unconstrained RP and TA (TMP-J) scenario. The analytical approximation results have been validated by numerically-obtained global-optimal solutions as well as via extensive Monte-Carlo simulations. Our results show that TMP-RP, TMP-TA, and TMP-J offer respectively about 30%, 75%, and 200% more gain with respect to fixed TA-RP scheme in terms of achievable throughput for a given EH requirement at the source and destination. In light of the projected RF-EH technology growth, we have also discussed significance of the considered system architecture towards green communication system. We believe that the results in this paper will provide a benchmark for the realization of perpetual operation of IoT and relay-assisted machine-to-machine communications.

Appendix A
Proof of Theorem 1

Here we prove generalized-convexity of TMP-TA by showing pseudoconcavity of its objective in ρ_2, followed by convexity of $C9$–$C11$ and global-optimality of the KKT point.

Pseudoconcavity of τ in ρ_2: Using (13), (12), and definitions of CCDF $\overline{F_{\gamma_{\mathcal{S}\mathcal{R}}}}$ and $\overline{F_{\gamma_{\mathcal{R}\mathcal{D}}}}$ of $\gamma_{\mathcal{S}\mathcal{R}}$ and $\gamma_{\mathcal{R}\mathcal{D}}$, respectively given in Lemmas 2 and 3, $\tau = R\left(\overline{F_{\gamma_{\mathcal{S}\mathcal{R}}}}\right)\left(\overline{F_{\gamma_{\mathcal{R}\mathcal{D}}}}\right)$. As log-concavity of $\overline{F_{\gamma_{\mathcal{R}\mathcal{D}}}}$ in ρ_2 is proved in Lemma 3, we next prove pseudoconcavity of $\overline{F_{\gamma_{\mathcal{S}\mathcal{R}}}}$ in ρ_2.

Lemma 2: The CCDF of the received SNR $\gamma_{\mathcal{S}\mathcal{R}}$ at $\mathcal{R}$ is pseudoconcave function of TA ρ_2.

Proof: The CCDF $\overline{F_{\gamma_{\mathcal{S}\mathcal{R}}}}$ of $\gamma_{\mathcal{S}\mathcal{R}}$, which is defined as: $\overline{F_{\gamma_{\mathcal{S}\mathcal{R}}}} \triangleq \Pr\left[\gamma_{\mathcal{S}\mathcal{R}} > 2^{\frac{R}{\rho_2}} - 1\right]$ can be obtained from (11) and (12). First, we prove the log-concavity of $\overline{F_{\gamma_{\mathcal{S}\mathcal{R}}}}$ in ρ_2 by showing its unimodality. The critical point or mode (maxima) of $\overline{F_{\gamma_{\mathcal{S}\mathcal{R}}}}$ in ρ_2, i.e., $\frac{\partial \overline{F_{\gamma_{\mathcal{S}\mathcal{R}}}}}{\partial \rho_2} = 0$, is obtained by solving (A.1).

$$\frac{2^{\frac{R}{\rho_2}} R \ln(2)\left(1-\rho_{ET}^{*}-2\rho_2\right) - \rho_2\left(1-\rho_{ET}^{*}\right)\left(2^{\frac{R}{\rho_2}}-1\right)}{\left[\mathcal{Z}\,\mathbf{K_0}\left(\mathcal{Z}\right)\right]^{-1}\rho_2\left(1-\rho_{ET}^{*}-2\rho_2\right)^2} = 0 \tag{A.1}$$

where $\mathcal{Z} = \mathcal{C}_1 \left(d_{\mathcal{S}\mathcal{R}}\right)^{\mathcal{B}\alpha}\left(\frac{\rho_2\left(2^{\frac{R}{\rho_2}}-1\right)}{1-2\rho_2-\rho_{ET}^{*}}\right)^{\frac{\mathcal{B}}{2}}$. The solution of (A.1) is: $\rho_2 = \widehat{\rho_{2,C}} \triangleq \frac{\left(1-\rho_{ET}^{*}\right)}{2+\frac{\left(1-\rho_{ET}^{*}\right)}{R\ln(2)}\left[\mathbf{W}\left(-4^{-\frac{R}{1-\rho_{ET}^{*}}}\,e^{-1}\right)+1\right]}$ with $\mathbf{W}(\cdot)$ as the Lambert function [37]. If $\rho_2 > \widehat{\rho_{2,C}}$, $\frac{\partial \overline{F_{\gamma_{\mathcal{S}\mathcal{R}}}}}{\partial \rho_2} < 0$. Otherwise if $\rho_2 < \widehat{\rho_{2,C}}$, then $\frac{\partial \overline{F_{\gamma_{\mathcal{S}\mathcal{R}}}}}{\partial \rho_2} > 0$. As unimodality of a single variable function is equivalent to its pseudoconcavity [39, Propositions 3.8 and 3.27], this proves that $\overline{F_{\gamma_{\mathcal{S}\mathcal{R}}}}$ is unimodal and pseudoconcave function of ρ_2. ■

Lemma 3: The CCDF of received SNR $\gamma_{\mathcal{R}\mathcal{D}}$ at $\mathcal{D}$ in i^{2}RES-assisted RF-EH communication over Rician channels is log-concave in both TA ρ_2 and RP $d_{\mathcal{S}\mathcal{R}}$ with $d_{\mathcal{R}\mathcal{D}} = D + \delta - d_{\mathcal{S}\mathcal{R}}$.

Proof: Log-concavity of a function can be proved by showing concavity of log of that function [36], [39]. Using (10) and (12), we observe that CCDF $\overline{F_{\gamma_{\mathcal{R}\mathcal{D}}}} \triangleq \Pr\left[\gamma_{\mathcal{R}\mathcal{D}} > 2^{\frac{R}{\rho_2}} - 1\right]$ of received SNR at $\mathcal{D}$ is log-concave in ρ_2, because $\frac{\partial^2 \ln\left(\overline{F_{\gamma_{\mathcal{R}\mathcal{D}}}}\right)}{\partial \rho_2^2}$, as defined in (A.2), is strictly negative for $\mathcal{B} > 1$:

$$\frac{\partial^2 \ln\left(\overline{F_{\gamma_{\mathcal{R}\mathcal{D}}}}\right)}{\partial \rho_2^2} = \frac{-\left[R\ln(2)\left(2^{\frac{R}{\rho_2}}\mathcal{B}-1\right)+2\rho_2\left(2^{\frac{R}{\rho_2}}-1\right)\right]}{\left[2^{\frac{R}{\rho_2}}\mathcal{B}R\mathcal{C}_2\ln(2)\left(d_{\mathcal{R}\mathcal{D}}\right)^{\mathcal{B}\alpha}\right]^{-1}\rho_2^4\left(2^{\frac{R}{\rho_2}}-1\right)^{2-\mathcal{B}}} \tag{A.2}$$

Similarly, the log-concavity of $\overline{F_{\gamma_{\mathcal{R}\mathcal{D}}}}$ in RP $d_{\mathcal{S}\mathcal{R}}$ with $d_{\mathcal{R}\mathcal{D}} = D + \delta - d_{\mathcal{S}\mathcal{R}}$ can be proved by showing that $\frac{\partial^2 \ln\left(\overline{F_{\gamma_{\mathcal{R}\mathcal{D}}}}\right)}{\partial d_{\mathcal{S}\mathcal{R}}^2} = -\frac{\mathcal{B}\alpha\mathcal{C}_2(\mathcal{B}\alpha-1)\left(2^{\frac{R}{\rho_2}}-1\right)^{\mathcal{B}}}{\left[\left(D+\delta-d_{\mathcal{S}\mathcal{R}}\right)^{\mathcal{B}\alpha-2}\right]^{-1}} < 0$. This completes the proof. ■

Applying [21, Lemma 5] in Lemma 3 given above, we can show that a positive differentiable log-concave function $\overline{F_{\gamma_{\mathcal{R}\mathcal{D}}}}$ is also pseudoconcave in ρ_2. Finally, using the individual pseudoconcavity of $\overline{F_{\gamma_{\mathcal{S}\mathcal{R}}}}$ and $\overline{F_{\gamma_{\mathcal{R}\mathcal{D}}}}$ in ρ_2, along with the result that product of two positive pseudoconcave functions is pseudoconcave [39], we have proved the pseudoconcavity of τ in ρ_2 for $R > 0$.

Convexity of $C9$–$C11$: The function corresponding to $C9$, $\mathcal{F}_{C9}(\rho_2) \triangleq \frac{\left(1-2\rho_2-\rho_{ET}^{*}\right)\eta_{\mathcal{S}}\, a_{\mathcal{R}\mathcal{S}}\, P_{\mathcal{R}}\, G_{\mathcal{R}}\, G_{\mathcal{S}}^2}{\rho_2\left(d_{\mathcal{S}\mathcal{R}}\right)^{\alpha}\mathcal{Y}\,\mathrm{EIRP}_{\max}} - 1$, is convex in ρ_2

because $\frac{\partial^2 \mathcal{F}_{C9}}{\partial \rho_2^2} = \frac{2\left(1-\rho_{ET}^*\right)\eta_{\mathcal{S}}\, a_{\mathcal{RS}}\, P_{\mathcal{R}}\, G_{\mathcal{R}}\, G_{\mathcal{S}}^2}{\rho_2^3 \left(d_{\mathcal{SR}}\right)^{\alpha} \mathcal{Y}\, \mathrm{EIRP}_{\max}} \geq 0 \quad \forall \rho_{ET}^* \leq 1$ (feasibility condition (23) for TMP-TA). Remaining two constraints $C10$–$C11$ are affine (or convex) functions of ρ_2.

Global-Optimality of the KKT Point in TMP-TA: As the objective function τ of TMP-TA is pseudoconcave in ρ_2 and constraints $C9$–$C11$ are differentiable and convex, on using [36, Theorem 4.3.8] it can be shown that KKT point of TMP-TA yields the global-optimal solution.

Appendix B
Proof of Theorem 2

Before proving generalized-convexity of TMP-RP, we present the following useful results.

Lemma 4: A positive non-increasing log-concave transformation $\Phi(\cdot)$ of a positive convex function $\Psi(\cdot)$ is log-concave, i.e., composition $(\Phi \circ \Psi)$ is log-concave.

Proof: As $\Psi(x)$ is a convex function of x, $\Psi''(x) = \frac{\partial^2 \Psi(x)}{\partial x^2} \geq 0$. Similarly, non-increasing log-concave [39], [40] transformation $\Phi(x)$ implies that $\frac{\partial^2 \ln(\Phi(x))}{\partial x^2} = \frac{\Phi''(x)}{\Phi(x)} - \left(\frac{\Phi'(x)}{\Phi(x)}\right)^2 \leq 0$ and $\Phi'(x) = \frac{\partial \Phi(x)}{\partial x} \leq 0$. To prove log-concavity of $(\Phi \circ \Psi)(x)$, we next show that $\frac{\partial^2 \ln(\Phi(\Psi(x)))}{\partial x^2} \leq 0$.

$$\frac{\partial^2 \ln\left(\Phi\left(\Psi\left(x\right)\right)\right)}{\partial x^2} = \frac{\left[\Psi'(x)\right]^2 \Phi''(\Psi(x))}{\Phi(\Psi(x))} - \frac{\left[\Psi'(x)\right]^2 \left[\Phi'(\Psi(x))\right]^2}{\left[\Phi(\Psi(x))\right]^2} + \frac{\Psi''(x)\Phi'(\Psi(x))}{\Phi(\Psi(x))}. \tag{B.1}$$

On applying log-concavity of the transformation $\Phi(\cdot)$ in (B.1), it is observed that the difference of first and second terms is non-positive, i,e., $\left[\Psi'(x)\right]^2 \left(\frac{\Phi''(\Psi(x))}{\Phi(\Psi(x))} - \left[\frac{\Phi'(\Psi(x))}{\Phi(\Psi(x))}\right]^2\right) \leq 0$, Further, the third term $\frac{\Psi''(x)\Phi'(\Psi(x))}{\Phi(\Psi(x))}$ in (B.1) is non-positive because $\Psi''(x)$ is non-negative due to convexity of Ψ, $\Phi'(\Psi(x))$ is non-positive due to non-increasing nature of Φ, and $\Phi(\Psi(x))$ is a positive transformation. This proves that $\frac{\partial^2 \ln(\Phi(\Psi(x)))}{\partial x^2} \leq 0$ and composition $(\Phi \circ \Psi)$ is log-concave. ■

Lemma 5: CCDF of received SNR $\gamma_{\mathcal{SR}}$ at $\mathcal{R}$ in proposed model is log-concave in RP $d_{\mathcal{SR}}$.

Proof: Using the definition given in Lemma 2, we consider $\overline{F_{\gamma_{\mathcal{SR}}}} = (\Phi \circ \Psi)$ as a composite function, where $\Phi(x) = x\, \mathbf{K_1}(x)$ and $\Psi\left(d_{\mathcal{SR}}\right) = \mathcal{C}_1 \left(d_{\mathcal{SR}}\right)^{\mathcal{B}\alpha} \left(\frac{\rho_2\left(2^{\frac{R}{\rho_2}}-1\right)}{1-2\rho_2-\rho_{ET}^*}\right)^{\frac{\mathcal{B}}{2}}$. Strict-convexity of Ψ in $d_{\mathcal{SR}}$ can be observed from the fact that: $\frac{\partial^2 \Psi}{\partial d_{\mathcal{SR}}^2} = \mathcal{B}\alpha\left(\mathcal{B}\alpha - 1\right)\mathcal{C}_1 \left(d_{\mathcal{SR}}\right)^{-2} \Psi\left(d_{\mathcal{SR}}\right) > 0$.

Regarding the properties of $\Phi(x) = x\, \mathbf{K_1}(x)$, we note that it is a bounded positive non-increasing function, where $0 \leq x\, \mathbf{K_1}(x) \leq 1$. Next we prove the log-concavity of $\Phi(x)$.

$$\frac{\partial^2 \ln(\Phi(x))}{\partial x^2} = \frac{\partial^2 \ln(x\, \mathbf{K_1}(x))}{\partial x^2} = 1 - \frac{\mathbf{K_0}(x)}{x\, \mathbf{K_1}(x)} - \left(\frac{\mathbf{K_0}(x)}{\mathbf{K_1}(x)}\right)^2 \tag{B.2}$$

With $x > 0$, as $\mathbf{K_1}(x) > 0$ and $0 \leq x\, \mathbf{K_1}(x) \leq 1$, negativity of (B.2) requires that if $\frac{\mathbf{K_0}(x)}{\mathbf{K_1}(x)} \leq \frac{\sqrt{[\mathbf{K_1}(x)]^2+4}-\mathbf{K_1}(x)}{2}$, then $x < \frac{\mathbf{K_0}(x)\mathbf{K_1}(x)}{[\mathbf{K_1}(x)]^2-[\mathbf{K_0}(x)]^2}$, which can be easily observed to be always true. Thus, we showed that composition function $\overline{F_{\gamma_{\mathcal{SR}}}}$ is a positive non-increasing log-concave transformation $\Phi(\cdot)$ of a positive convex function $\Psi\left(d_{\mathcal{SR}}\right)$. This along with Lemma 4 proves that $\overline{F_{\gamma_{\mathcal{SR}}}}$ is log-concave in RP $d_{\mathcal{SR}}$. ■

Using the above results from Lemmas 4, 3, and 5, pseudo-concavity of τ in $d_{\mathcal{SR}}$ for a fixed TA can be proved in three steps. First, using Lemmas 3 and 5, we show that CCDF of both $\gamma_{\mathcal{SR}}$ and $\gamma_{\mathcal{RD}}$ are log-concave in $d_{\mathcal{SR}}$. Second, by using the property that log-concavity is preserved under positive product [35], [40], we show that τ, which is a positive product of $\overline{F_{\gamma_{\mathcal{SR}}}}$ and $\overline{F_{\gamma_{\mathcal{RD}}}}$, is log-concave in $d_{\mathcal{SR}}$. Finally from [21, Lemma 5], we show that a positive differentiable log-concave function τ is pseudoconcave in $d_{\mathcal{SR}}$. Apart from this, the convexity of box constraints $d_{\mathrm{LB}} \leq d_{\mathcal{SR}}$ and $d_{\mathcal{SR}} \leq d_{\mathrm{UB}}$, proves the generalized-convexity of TMP-RP.

Appendix C
Proof of Theorem 3

The joint-pseudoconcavity of τ, objective function of TMP-J, in ρ_2 and $d_{\mathcal{SR}}$ is proved in three steps. First, from Lemma 3 we observe that $\overline{F_{\gamma_{\mathcal{RD}}}}$ is a strictly-increasing as well as strictly log-concave (or strictly-pseudoconcave using positivity of $\overline{F_{\gamma_{\mathcal{RD}}}}$ and [21, Lemma 5]) function of both ρ_2 and $d_{\mathcal{SR}}$. Using this result along with the property that product of two positive strictly-pseudoconcave function is also pseudoconcave [39], we prove joint-pseudoconcavity of $\overline{F_{\gamma_{\mathcal{RD}}}}$ in ρ_2 and $d_{\mathcal{SR}}$. Second, we prove joint-pseudoconcavity of $\overline{F_{\gamma_{\mathcal{SR}}}}$ in ρ_2 and $d_{\mathcal{SR}}$ using Lemma 6 which presented at the end of this Appendix. Using the above two steps along with pseudoconcavity preserving property of a positive product in $\tau = R\left(\overline{F_{\gamma_{\mathcal{SR}}}}\right)\left(\overline{F_{\gamma_{\mathcal{RD}}}}\right)$, joint-pseudoconcavity of τ in ρ_2 and $d_{\mathcal{SR}}$ can be observed for $R > 0$.

Lemma 6: The CCDF of received SNR $\gamma_{\mathcal{SR}}$ at $\mathcal{R}$ is jointly-pseudoconcave in ρ_2 and $d_{\mathcal{SR}}$.

Proof: We define $g_1 \triangleq \rho_2\left(2^{\frac{R}{\rho_2}}-1\right)$, $g_2 \triangleq \frac{\left(d_{\mathcal{SR}}\right)^{2\mathcal{B}\alpha}}{1-2\rho_2-\rho_{ET}^*}$, such that $\overline{F_{\gamma_{\mathcal{SR}}}} = \mathbf{K_1}\left(\mathcal{C}_1 \left(g_1 g_2\right)^{\frac{\mathcal{B}}{2}}\right)\mathcal{C}_1 \left(g_1 g_2\right)^{\frac{\mathcal{B}}{2}}$. As $\frac{\partial g_1}{\partial \rho_2^2} = \frac{2^{\frac{R}{\rho_2}}\left[R\ln(2)\right]^2}{\rho_2^3} > 0$, and g_1 is independent of $d_{\mathcal{SR}}$, we claim that g_1 is jointly and strictly-convex in ρ_2 and $d_{\mathcal{SR}}$. Next we prove the joint strict-convexity of g_2 by observing that $\frac{\partial^2 g_2}{\partial \rho_2^2} = \frac{8\left(d_{\mathcal{SR}}\right)^{2\mathcal{B}\alpha}}{\left(\widehat{\rho_1}\right)^3} > 0$, $\frac{\partial^2 g_2}{\partial d_{\mathcal{SR}}^2} = \frac{d_{\mathcal{SR}}^{2\mathcal{B}\alpha}}{\left(\widehat{\rho_1}\right)^3}\Bigg[2\left(\mathcal{B}\alpha\right)^2 \times \left(\frac{\zeta_{E\mathcal{D}}\left(d_{\mathcal{RD}}\right)^{\alpha-1}}{\eta_{\mathcal{D}}\, a_{\mathcal{RD}}\, G_{\mathcal{R}}\, G_{\mathcal{D}}\, P_{\mathcal{R}}} - \frac{\zeta_{E\mathcal{S}}\left(d_{\mathcal{SR}}\right)^{\alpha-1}}{\eta_{\mathcal{S}}\, a_{\mathcal{RS}}\, P_{\mathcal{R}}\, G_{\mathcal{R}}\, G_{\mathcal{S}}} - \frac{\widehat{\rho_1}}{d_{\mathcal{SR}}}\right)^2 + \frac{\alpha(\mathcal{B}\alpha-1)\left(\widehat{\rho_1}\right)^2}{[2\mathcal{B}]^{-1} d_{\mathcal{SR}}^2} + \left(\frac{\zeta_{E\mathcal{D}}\left(d_{\mathcal{RD}}\right)^{\alpha-2}}{\eta_{\mathcal{D}}\, a_{\mathcal{RD}}\, G_{\mathcal{R}}\, G_{\mathcal{D}}\, P_{\mathcal{R}}} + \frac{\zeta_{E\mathcal{S}}\left(d_{\mathcal{SR}}\right)^{\alpha-2}}{\eta_{\mathcal{S}}\, a_{\mathcal{RS}}\, P_{\mathcal{R}}\, G_{\mathcal{R}}\, G_{\mathcal{S}}}\right)\alpha(\alpha-1)\widehat{\rho_1}\Bigg] > 0$, and determinant of Hessian matrix of g_2 is: $\frac{8(\mathcal{B}\alpha-1)\left(d_{\mathcal{SR}}\right)^{4\mathcal{B}\alpha}}{[\mathcal{B}\alpha]^{-1}\left(\widehat{\rho_1}\right)^5} \times \left(\frac{d_{\mathcal{RD}}}{d_{\mathcal{SR}}}\right)^2 \left(2\widehat{\rho_1} + \frac{\zeta_{E\mathcal{S}}\left(d_{\mathcal{SR}}\right)^{\alpha}}{\eta_{\mathcal{S}}\, a_{\mathcal{RS}}\, P_{\mathcal{R}}\, G_{\mathcal{R}}\, G_{\mathcal{S}}} + \frac{\zeta_{E\mathcal{D}}\, d_{\mathcal{SR}}^2\left(d_{\mathcal{RD}}\right)^{\alpha-2}}{\eta_{\mathcal{D}}\, a_{\mathcal{RD}}\, G_{\mathcal{R}}\, G_{\mathcal{D}}\, P_{\mathcal{R}}}\right) > 0, \forall\left(\widehat{\rho_1} > 0\right) \wedge \left(\alpha > \frac{3}{2}\right) \wedge \left(d_{\mathcal{RD}} = D + \delta - d_{\mathcal{SR}}\right)$. This proves strict joint-convexity of g_2 in ρ_2 and $d_{\mathcal{SR}}$. As product of two positive strictly-convex functions is pseudoconvex [39], we are able to show that $g_1 g_2$ is jointly-pseudoconvex in ρ_2 and $d_{\mathcal{SR}}$. Also, as $\mathcal{C}_1 x^{\frac{\mathcal{B}}{2}}\ \mathbf{K_1}\left(\mathcal{C}_1 x^{\frac{\mathcal{B}}{2}}\right)$ is a strictly decreasing function of x for $\mathcal{C}_1 > 0$, $\mathcal{B} > 1$, and non-increasing transformation of a pseudoconvex function is pseudoconcave [35], we show that $\overline{F_{\gamma_{\mathcal{SR}}}}$ is jointly-pseudoconcave in ρ_2 and $d_{\mathcal{SR}}$. ■

REFERENCES

[1] X. Lu *et al.*, "Wireless charging technologies: Fundamentals, standards, and network applications," *IEEE Commun. Surveys Tuts.*, vol. 18, no. 2, pp. 1413–1452, Secondquarter 2016.

[2] D. Mishra *et al.*, "Smart RF energy harvesting communications: Challenges and opportunities," *IEEE Commun. Mag.*, vol. 53, no. 4, pp. 70–78, Apr. 2015.

[3] P.-H. Hsieh, C.-H. Chou, and T. Chiang, "An RF energy harvester with 44.1% PCE at input available power of -12 dbm," *IEEE Trans. Circuits Syst. I, Reg. Papers*, vol. 62, no. 6, pp. 1528–1537, June 2015.

[4] Z. Ding *et al.*, "Application of smart antenna technologies in simultaneous wireless information and power transfer," *IEEE Commun. Mag.*, vol. 53, no. 4, pp. 86–93, Apr. 2015.

[5] P. Kamalinejad *et al.*, "Wireless energy harvesting for the internet of things," *IEEE Commun. Mag.*, vol. 53, no. 6, pp. 102–108, June 2015.

[6] D. Mishra and S. De, "Optimal relay placement in two-hop RF energy transfer," *IEEE Trans. Commun.*, vol. 63, no. 5, pp. 1635–1647, May 2015.

[7] X. Huang and N. Ansari, "Energy sharing within EH-enabled wireless communication networks," *IEEE Wireless Commun.*, vol. 22, no. 3, pp. 144–149, June 2015.

[8] S. Ulukus *et al.*, "Energy harvesting wireless communications: A review of recent advances," *IEEE J. Sel. Areas Commun.*, vol. 33, no. 3, pp. 360–381, Mar. 2015.

[9] H. Ju and R. Zhang, "Throughput maximization in wireless powered communication networks," *IEEE Trans. Wireless Commun.*, vol. 13, no. 1, pp. 418–428, Jan. 2014.

[10] H. Chen *et al.*, "Harvest-then-cooperate: Wireless-powered cooperative communications," *IEEE Trans. Signal Process.*, vol. 63, no. 7, pp. 1700–1711, Apr. 2015.

[11] I. Krikidis *et al.*, "Simultaneous wireless information and power transfer in modern communication systems," *IEEE Commun. Mag.*, vol. 52, no. 11, pp. 104–110, Nov. 2014.

[12] D. Mishra and S. De, "Optimal time allocation for RF-powered DF relay-assisted cooperative communication," *IET Electron. Lett.*, vol. 52, no. 14, pp. 1274–1276(2), July 2016.

[13] Z. Hadzi-Velkov *et al.*, "Rate maximization of decode-and-forward relaying systems with RF energy harvesting," *IEEE Commun. Lett.*, vol. 19, no. 12, pp. 2290–2293, Dec. 2015.

[14] S. Lohani *et al.*, "On multiuser resource allocation in relay-based wireless-powered uplink cellular networks," *IEEE Trans. Wireless Commun.*, vol. 15, no. 3, pp. 1851–1865, Mar. 2016.

[15] K. Huang and V. Lau, "Enabling wireless power transfer in cellular networks: Architecture, modeling and deployment," *IEEE Trans. Wireless Commun.*, vol. 13, no. 2, pp. 902–912, Feb. 2014.

[16] G. Huang, Q. Zhang, and J. Qin, "Joint time switching and power allocation for multicarrier decode-and-forward relay networks with SWIPT," *IEEE Signal Process. Lett.*, vol. 22, no. 12, pp. 2284–2288, Dec. 2015.

[17] Z. Zhou *et al.*, "Joint power splitting and antenna selection in energy harvesting relay channels," *IEEE Signal Process. Lett.*, vol. 22, no. 7, pp. 823–827, July 2015.

[18] Y. Huang and B. Clerckx, "Joint wireless information and power transfer for an autonomous multiple antenna relay system," *IEEE Commun. Lett.*, vol. 19, no. 7, pp. 1113–1116, July 2015.

[19] A. Nasir *et al.*, "Relaying protocols for wireless energy harvesting and information processing," *IEEE Trans. Wireless Commun.*, vol. 12, no. 7, pp. 3622–3636, July 2013.

[20] G. Zhu *et al.*, "Wireless information and power transfer in relay systems with multiple antennas and interference," *IEEE Trans. Commun.*, vol. 63, no. 4, pp. 1400–1418, Apr. 2015.

[21] D. Mishra, S. De, and C.-F. Chiasserini, "Joint optimization schemes for cooperative wireless information and power transfer over rician channels," *IEEE Trans. Commun.*, vol. 64, no. 2, pp. 554–571, Feb. 2016.

[22] Z. Ding *et al.*, "Wireless information and power transfer in cooperative networks with spatially random relays," *IEEE Trans. Wireless Commun.*, vol. 13, no. 8, pp. 4440–4453, Aug. 2014.

[23] H. Tabassum and E. Hossain, "On the deployment of energy sources in wireless-powered cellular networks," *IEEE Trans. Commun.*, vol. 63, no. 9, pp. 3391–3404, Sep. 2015.

[24] S. Bi and R. Zhang, "Placement optimization of energy and information access points in wireless powered communication networks," *IEEE Trans. Wireless Commun.*, vol. 15, no. 3, pp. 2351–2364, Mar. 2016.

[25] M. Bocus, C. Dettmann, and J. Coon, "An approximation of the first order Marcum Q-function with application to network connectivity analysis," *IEEE Commun. Lett.*, vol. 17, no. 3, pp. 499–502, Mar. 2013.

[26] A. Goldsmith, *Wireless communications*. Cambridge University Press, 2005.

[27] M. K. Simon and M.-S. Alouini, *Digital communication over fading channels*, 2nd ed. New York, USA: Wiley, 2005.

[28] S. Lee, L. Liu, and R. Zhang, "Collaborative wireless energy and information transfer in interference channel," *IEEE Trans. Wireless Commun.*, vol. 14, no. 1, pp. 545–557, Jan 2015.

[29] W. Huang *et al.*, "On the performance of multi-antenna wireless-powered communications with energy beamforming," *IEEE Trans. Veh. Technol.*, vol. 65, no. 3, pp. 1801–1808, Mar. 2016.

[30] Y. Gu *et al.*, "A discrete time-switching protocol for wireless-powered communications with energy accumulation," in *Proc. IEEE GLOBECOM*, San Diego, Dec. 2015, pp. 1–6.

[31] I. Akyildiz and X. Wang, *Wireless mesh networks*. John Wiley & Sons, 2009, vol. 3.

[32] I. Krikidis, "Simultaneous information and energy transfer in large-scale networks with/without relaying," *IEEE Trans. Commun.*, vol. 62, no. 3, pp. 900–912, Mar. 2014.

[33] Federal Communications Commission (FCC), "Rules and regulations," *Federal Register*, vol. 79, no. 84, pp. 24 569–24 580, May 2014.

[34] C. A. Balanis, *Antenna theory: analysis and design*. John Wiley & Sons, 2012.

[35] A. Cambini and L. Martein, *Generalized convexity and optimization: Theory and applications*. Springer, 2008, vol. 616.

[36] M. S. Bazaraa, H. D. Sherali, and C. M. Shetty, *Nonlinear Programming: Theory and Applications*. New York: John Wiley and Sons, 2006.

[37] E. W. Weisstein, "Lambert W-Function," From MathWorld – A Wolfram Web Resource. [Online]. Available: http://mathworld.wolfram.com/LambertW-Function.html

[38] C. Zhong *et al.*, "Wireless information and power transfer with full duplex relaying," *IEEE Trans. Commun.*, vol. 62, no. 10, pp. 3447–3461, Oct. 2014.

[39] M. Avriel *et al.*, *Generalized concavity*. Philadelphia, PA, USA: SIAM, vol. 63, 2010.

[40] A. Prékopa, "Logarithmic concave measures and related topics," in *Stochastic programming*. London: Academic Press, M. A. H. Dempster, Ed., 1980, pp. 63–82.

Deepak Mishra (S'13) received his B.Tech degree in Electronics and Communication Engineering from Guru Gobind Singh Indraprastha University, Delhi, India, in 2012. He is currently pursuing the Ph.D. degree from the Department of Electrical Engineering, IIT Delhi, India. He is a recipient 2016 IBM Ph.D. Fellowship award. His research interests include energy harvesting cooperative communication networks and energy optimization schemes for uninterrupted operation of mobile ad hoc networks.

Swades De (S'02-M'04-SM'14) received the Ph.D. degree from the State University of New York at Buffalo, NY, USA, in 2004. From 1993 to 1997 and in 1999, he worked in different communication companies in India as a research and development engineer. During the first half of 2004 he worked with the wireless networks group at ISTI-CNR, in Pisa, Italy, through ERCIM fellowship. From 2004 to 2006 he was with the New Jersey Institute of Technology, USA, as a Tenure-Track Assistant Professor of Electrical and Computer Engineering. He joined the Department of Electrical Engineering at Indian Institute of Technology Delhi in 2007, where he is currently an Associate Professor. His research interests are broadly in communication networks, with emphasis on performance modeling and analysis. Current directions include energy harvesting communication networks, broadband wireless access and routing, cognitive/white-space access networks, and smart grid networks.

Dr. De is a Senior Member of IEEE, a Member of IEICE Japan, and a Fellow of the Indian National Academy of Engineering. Currently he serves as a Senior Editor of IEEE Communications Letters and Associate Editor respectively of Springer Photonic Network Communications journal and IETE Technical Review journal.